FOSSIL EVIDENCE FOR THE RECENT DEVELOPMENT OF HYPOXIA ON THE TEXAS SHELF FROM SEDIMENTARY RECORDS

A Thesis

by

CALIE RAI PAYNE

Submitted to the Graduate and Professional School of
Texas A&M University
in partial fulfillment of the requirements for the degree of

MASTER OF SCIENCE

Chair of Committee,	Christina Belanger
Committee Members,	Ethan Grossman
	Timothy Dellapenna
Head of Department,	Julie Newman

August 2021

Major Subject: Geology

ABSTRACT

Since the 1950s, low-oxygen (hypoxic) conditions have developed in the northern Gulf of Mexico (GoM) due to increased nutrient flux from the Mississippi River. Despite the threat hypoxia poses to profitable fisheries and the extensive studies of the Louisiana Shelf, few studies have examined hypoxia on the Texas Shelf. Low-oxygen conditions on the Texas Shelf may be driven by regional processes such as the western migration of freshwater from the Mississippi–Atchafalaya plume, and thus linked to the Mississippi River nutrient fluxes, or driven by local processes like freshwater runoff and, thus, developed independently. Here, I use variation in benthic foraminiferal faunas from ^{210}Pb-dated sedimentary cores to assess the temporal extent and severity of hypoxia on the Texas Shelf over the past ~150 years for comparison with Louisiana Shelf studies. Benthic foraminifera are sensitive to oxygen levels, and assemblages from surface sediments reflect present-day hypoxic conditions near Port Aransas, Texas. I reconstructed oxygenation over the past ~150 years in two sediment cores near Port Aransas using the full faunal assemblages and three benthic foraminiferal oxygenation proxies: the PEB index based upon the relative abundance of three hypoxia-tolerant foraminifers (*Pseudononion atlanticum*, *Epistominella vitrea*, and *Buliminella morgani*), the PEBn index (PEB taxa + *Nonionella opima*), and the A-E index based upon the relative dominance of *Ammonia* to *Elphidium* species. Additionally, I integrated oxygen and carbon isotope measurements performed on *Elphidium excavatum*, to examine shifts in salinity and organic matter remineralization in the sediments. Here, I found that hypoxic conditions have persisted on the Texas Shelf near Mustang Island since the ~1950s, as indicated by variation in the full faunal assemblages and the foraminiferal indices.

Secular increases in hypoxia may be related to Mississippi–Atchafalaya plume however the most extreme hypoxic events may be driven by Nueces River discharge during flooding events.

DEDICATION

This thesis is dedicated to my mother, Rhonda L. Payne (1963-2019), and nephew, Nixon C. Walker.

ACKNOWLEDGEMENTS

I would like to thank my thesis advisor and Chair of Committee, Dr. Christiania Belanger, for the endless amount of support. What I have learned from Dr. Belanger over the past 3.5 years has fostered my ability to approach research problems and tasks with confidence, providing me with a seamless transition from undergraduate to graduate research. Thank you to my committee members, Dr. Ethan Grossman, and Dr. Timothy Dellapenna, for their guidance and on-going support through an unprecedented time. Thank you to Dr. Christopher Lowery at the University of Texas for providing the sediment samples for this thesis. Thank you to Dr. David Bapst at Texas A&M University for guiding me through various statistical analyses that were used in this thesis. Thank you to all the micropaleontology graduate students working under Dr. Belanger who have provided guidance and support through my graduate research and coursework. Lastly, thank you to my dad and sister for the emotional support and encouragement while completing my M.S. during a period of mourning and the COVID-19 pandemic.

CONTRIBUTORS AND FUNDING SOURCES

This work was supervised by a thesis committee consisting of Professor Christina Belanger and Professor Ethan Grossman of the Department of Geology and Geophysics and Professor Timothy Dellapenna of the Department of Marine and Coastal Environmental Science.

The core samples for this thesis were provided by Professor Christopher Lowery of the Department of Geology and Geophysics at the University of Texas.

All other work conducted for the thesis was completed by the student independently.

NOMENCLATURE

AIC	Akaike Information Criterion
CTD	Conductivity, temperature and depth
GoM	Gulf of Mexico
GRW	General random walk
IAEA	International Atomic Energy Agency
M/A	Mississippi/Atchafalaya
N	Nitrogen
PC	Piston cores
PCO	Principal coordinate analysis
PIE	Probability of Interspecific Encounter
psu	practical salinity units
SAR	Sediment accumulation rate
SIGF	Stable Isotope Geosciences Facility
TAMU	Texas A&M University
TAMUG	Texas A&M University- Galveston
URW	Unbiased random walk

TABLE OF CONTENTS

LIST OF FIGURES

LIST OF TABLES

1. INTRODUCTION

Since the mid- 20th century, oxygen concentrations in coastal waters have declined and associated “dead zones" have spread exponentially (Diaz et al, 2008; Keeling et al., 2010; Stramma et al., 2008; Vaquer-Sunyer and Duarte, 2008). The “dead zone” is where coastal waters are depleted of dissolved oxygen concentrations (<2 mg O_2/L). Because nearly all metazoans require oxygen to survive, dead zones are detrimental to aquatic metazoan life. For example, the increased frequency and duration of extreme hypoxic conditions in shallower waters over the past century have caused a decline in coastal fisheries including the collapse of Gulf of Mexico brown shrimp (Smith et al., 2014; Purcell et al., 2017; Smith et al., 2017). Thus, understanding the historic conditions of Texas Shelf hypoxia is crucial for alleviating the effects low-oxygen waters pose on Texas fisheries in the future.

Expansion of dead zones in coastal regions are driven by two water column processes: eutrophication and stratification. Excessive nutrient influx, termed eutrophication, drives enhanced primary productivity, which then results in increased oxygen consumption in the bottom waters as organic matter is respired (Rabalais et al., 2007). In other cases, increased density-driven stratification hinders gas exchange between surface and bottom waters, preventing the re-oxygenation of bottom waters. Coastal waters are more vulnerable to density stratification relative to the open ocean because freshwater input via runoff inhibits the mixing between surface and deeper layers (DiMarco et al., 2012). Likewise, increased warming of shallow coastal waters can cause temperature-driven stratification between the warm surface waters and cool bottom waters, further reducing gas exchange (Keeling et al., 2010; Schmittner et al., 2008).

Although hypoxic conditions can occur naturally, the rise in hypoxia over the last century is largely due anthropogenic activities including agricultural and waste removal practices, artificial coastal modification (e.g. seawalls, groynes, jetties, etc.), and changes in land use (Rabalais et al., 2007; Zhang et al., 2010). Agricultural and waste removal practices release excessive nutrients into surface waters (also known as anthropogenically-induced eutrophication), in turn stimulating primary productivity and associated organic matter respiration. The global expansion of dead zones since the mid-20th century is synchronous with the human population tripling (United Nations Department of Social Affairs/Population Division, 2019) and global fertilizer increasing 10-fold over the same period (International Fertilizer Association, 2017). Thus, understanding the impact anthropogenic actions has on oxygen concentrations in coastal waters is crucial for alleviating the further expansion of dead zones and associated effects on aquatic ecosystems.

Paleo-records provide insight on what environments looked like prior to anthropogenic disturbance, allowing scientists and conservationists to establish environmental baselines. These baselines offer crucial information for conservationists and policy makers, especially when setting restoration and remediation goals. Benthic foraminifera, which are readily preserved in the marine sediment records, are a powerful tool for recording natural and anthropogenic perturbations in the modern oceans and throughout the paleooceanographic record (Murray, 2014). Different benthic foraminiferal species have different environmental preferences, thus the tests preserved in the sedimentary record can provide insight on what environments looked like prior to anthropogenic disturbance. Previous studies have compared faunal assemblages downcore to record the oxygenation history of the Louisiana Shelf since the 1950s (Nelsen et al.,

1994; Rabalais et al. 1996; Sen Gupta et al., 1996). These records provided the ability to link rising hypoxic conditions to increased nutrient loads from the Mississippi River.

In this study, I reconstruct the paleo-oxygen record of coastal Texas near Mustang Island – an understudied region – by analyzing total benthic foraminiferal assemblages from a nearshore and offshore core. If hypoxia has increased in this region since the 1950s, like the Louisiana Shelf, I expect an analogous increase in hypoxia-tolerant taxa. If density stratification due to freshwater runoff or warming of surface waters is the primary driver of hypoxia, I expect sites that are proximal to freshwater sources to indicate more severe hypoxia.

1.1. Northern Gulf of Mexico Hypoxia

The Gulf of Mexico (GoM) Dead Zone is located west of the Mississippi River along the Texas-Louisiana coast. This zone is the second largest anthropogenically-induced hypoxic area in the world, spanning approximately 23,000 km^2 in mid-summer at 5 to 60 m water depth (Rabalais et al., 2019). Coastal waters here are subject to freshwater discharge with high nutrient loads (primarily nitrogen and phosphorous) from the Mississippi River (Rabalais et al., 2020). This river drains 41% of the continental United States — primarily agricultural lands — delivering 10 times as much nitrate and phosphate to the ocean as any other major U.S. river (USGS, 2015; Figure 1-2). Since the 1950s, the total nitrogen (N) load in the Mississippi River discharge has increased significantly (David et al., 2010; USGS 2010). Nitrate loads increased from 200,000-500,000 t/yr in the 1950s and 1960s to ~1,000,000 t/yr during the 1980s and 1990s and decreased slightly to 900,000 t/yr since the 2000s (USGS, 2015; Figure 1). Multiple geological and biological paleo-hypoxia proxies suggest that low-oxygen conditions in the

northern Gulf of Mexico started during the 1950s, contemporaneously with increased nitrate loadings (Rabalais et al., 2007).

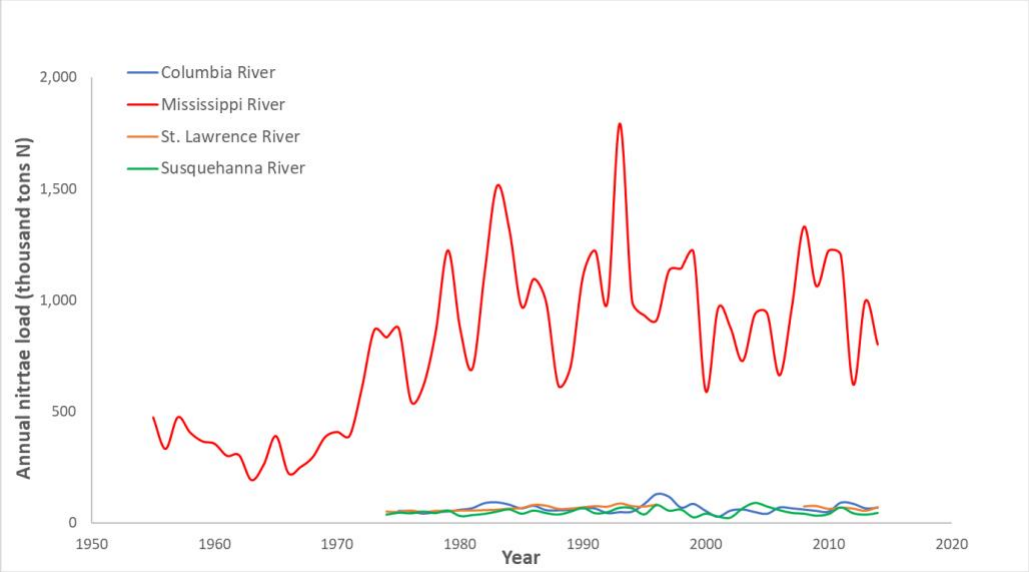

Figure 1. Nitrate loads in four major U.S. Rivers from 1955 to 2014. Data from USGS (2015).

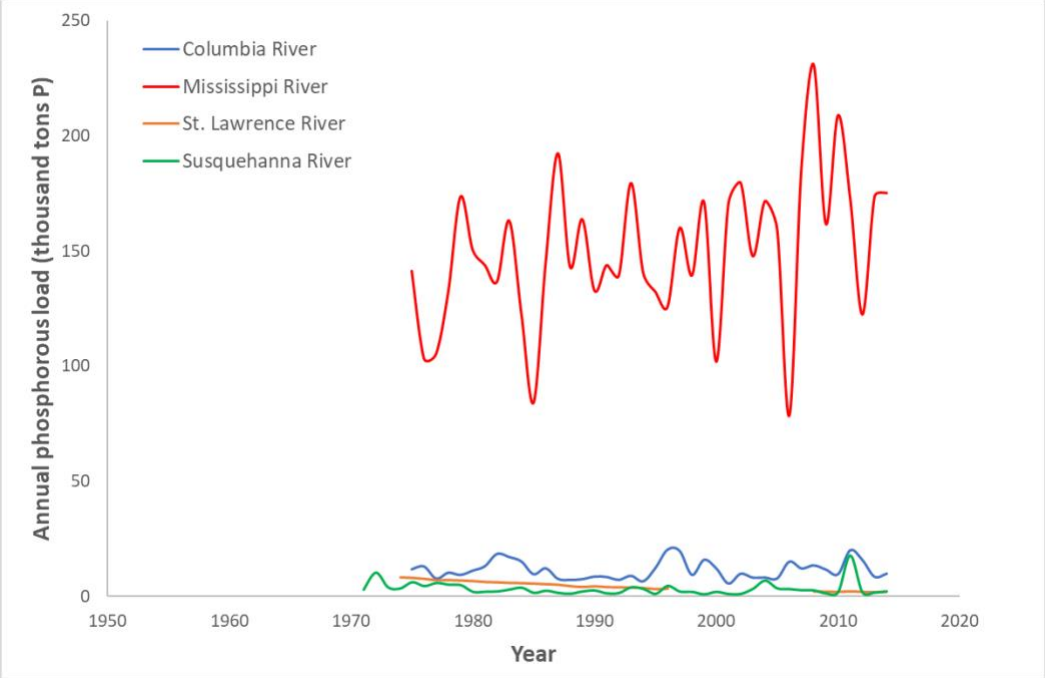

Figure 2. Total phosphorous loads in four major U.S. rivers from 1971 to 2014. Data

from USGS (2015).

Bottom-water oxygen concentrations in the northern GoM have been recorded annually since 1985 (Rabalis et al., 2002). The year-to-year trends show that the mid-summer bottom-area of dissolved oxygen on the Mississippi-Louisiana has increased, and occasionally extends into upper Texas coastal waters (Rabalais and Turner, 2019).

Decreased oxygenation in the northern GOM since the mid-century is recorded in the marine sedimentary record by three hypoxia indicators: (1) increased average abundance of glauconite in sediments (Nelsen et al. 1994), (2) decreased ostracod and foraminifera diversity (Nelsen et al. 1994), and (3) increase percent abundance of hypoxia-tolerant foraminiferal species (Rabalais et al. 1996; Sen Gupta, 1996; Rabalais et al., 2007). These hypoxia proxies are coincident with increased nitrate concentrations from fertilizer use in the Mississippi basin (Rabalais et al., 2007). Glauconite crystallizes under reducing conditions, thus an increased abundance of glauconite is indicative of low-oxygen conditions. From 1900 to 1950, the average proportion of glauconite in the coarse fraction of sediments was only 6%, but this increased to 13% from 1950 to 1990 (Nelsen et al. 1994). Ostracod and foraminiferal diversity decrease during periods of low-oxygen. In the northern GoM, foraminifera and ostracod diversity decreased from the 1940s to 1990s (Nelsen et al., 1994).

Most relevant to the study herein is the use of benthic foraminiferal assemblage composition as an oxygenation proxy. Benthic foraminifera are sensitive to environmental change and have been used as a low-oxygen bottom-water proxy in studies of coastal to deep-sea environments (Jorissen et al., 2007; Gooday et al., 2010). *Buliminella morgani*, a hypoxia-tolerant species, increased in abundance between 1950 and 1990 on the Louisiana Shelf (Rabalais et al. 1996). In addition to single indicator taxa, suites of hypoxia-tolerant foraminifers

are used to reconstruct the paleo-hypoxia record in the GoM. Sen Gupta et al. (1996) tracked an increase in hypoxia in Louisiana core sediments over the past 40 years using two foraminifera, *Ammonia* and *Elphidium*. Given *Ammonia* is more tolerant to hypoxic conditions than *E. excavatum*, they use the proportions of these foraminifers in a metric termed the A-E index:

$$\text{A} - \text{E Index} = \frac{N_A}{N_A + N_E} \times 100 \quad (1)$$

where N_A and N_E are the counts of *Ammonia* and *Elphidium*, respectively.

In the A-E index, a higher value, or higher portions of *Ammonia* relative to *Elphidium*, indicate hypoxia. The observed A-E values in past studies correlate with bottom water oxygenation (Thomas et al., 2000) and sedimentary organic matter (Sen Gupta et al., 1996), supporting the utility of this metric. Similarly, Osterman (2003) investigated present-day hypoxic conditions along the Louisiana-Texas coastline using benthic foraminiferal assemblage data (>125 μm size fraction) from 74 core-tops. She used multivariate analyses to summarize the variation in the relative abundances of benthic foraminiferal species and compared that variation to differences in water depth and oxygenation. The analyses distinguished a group of sites with similar faunal composition that was within the well-studied hypoxic zone off the Louisiana Shelf and several sites on the South Texas Shelf, suggesting low-oxygen conditions could be recognized in GoM via changes in the benthic foraminifera. Using these data, Osterman (2003) found that abundances of *P. atlanticum, E. vitrea and B. morgani* were high in hypoxic zones and defined the PEB index as:

$$\text{PEB index} = \frac{N_P + N_E + N_B}{N_T} \times 100 \quad (2)$$

where N_P, N_E, and N_B, are the counts of *P. atlanticum*, *E. vitrea*, *B. morgani*, respectively, and N_T is the total assemblage count.

The PEB index and A-E index are highest in hypoxic zones found on the Louisiana Shelf and Texas Shelf, consistent with modern hypoxic conditions in these regions (Osterman, 2003). Previous studies assessing the PEB index in core top samples suggest that modern-day hypoxia on the Texas Shelf occurs at 24 to 70 m between Galveston Island and Aransas Pass (Osterman, 2003), consistent with more recent instrumental measurements (May and NOAA Southeast Fisheries Science Center, 2011).

1.2. Texas Shelf Hypoxia

While hypoxia is intensely studied on the Louisiana Shelf, research regarding the oxygenation history on the Texas Shelf is sparse despite the potential for different drivers and historical patterns. Texas Shelf hypoxia is driven by water column stratification associated with either the western migration of Mississippi–Atchafalaya freshwater, intense local freshwater runoff, or a combination of both (DiMarco et al., 2012). The Mississippi–Atchafalaya discharge plume is concentrated along the Louisiana shelf and occasionally extends into upper Texas Shelf waters. However, during flooding events, such as the high flow of the Brazos River in 2007, Texas Shelf hypoxia was primarily driven by stratification due to the increase in freshwater discharge from the Brazos River, blocking the advancement of Mississippi–Atchafalaya freshwater (DiMarco et al., 2012). In 2008, during an interval of low flow for the Brazos River, the migration of freshwater from the Mississippi–Atchafalaya River System initiated hypoxic conditions instead. Thus, Texas Shelf hypoxia can be driven by water column stratification from either the Brazos River during high discharge or by Mississippi–Atchafalaya freshwater when flow from the Brazos River is normal to low (DiMarco et al., 2012).

Freshwater input to the coast can increase during natural flooding events; the average freshwater discharge of the Brazos River from 1941 to 2019 was ~ 7,795 $m^3 s^{-1}$, whereas past flooding events have caused discharge of up to 26,620 $m^3 s^{-1}$ (USGS River Gage 08114000, http:// waterdata.usgs.gov). In addition, changes in land use with urbanization (paving and excavation of soils) disrupts the natural hydrological processes of water catchments and reduces infiltration of water into soil (Suriya and Mudgal, 2011), causing urban watersheds to lose on average 90% of rainfall to runoff (Sheng and Wilson, 2009). These anthropogenic actions thus increase the volume of floodwater that reaches the continental shelf via runoff, which can drive water column stratification and associated hypoxia.

An increase in the frequency and magnitude of flooding events are linked to increased urbanization since the mid-20th century (Olivera and DeFee, 2007; Sheng and Wilson, 2009; Weng, 2001; Yang et al., 2014; Zhao and Gao, 2016). Since the 1910s the urban population of Texas increased from 24.1% to 84.7% as of 2010, making Texas the 3rd most urban state in the United States (White et al., 2017). Thus, if local runoff is the primary driver for Texas Shelf hypoxia, one would expect to see abrupt shifts in the record of Texas Shelf oxygenation record during the past century associated with major flooding events.

1.2.1. Urgency for Accessing Hypoxic Conditions Near Mustang Island, TX

Mustang Island is a Texas barrier island that separates the Corpus Christi Bay system from the open ocean. Aransas Pass (27.9095° N, 97.1506° W) is a tidal flat that connects Corpus Christi Bay to the Gulf of Mexico. This pass separates Mustang Island to the west from San Jose Island to the east. The Nueces River feeds into the Corpus Christi Bay system which consists of four secondary bays: Nueces Bay, Corpus Christi Bay, Oso Bay, and Redfish Bay. Since 1867, dredging of navigational channels, construction of jetties and other structural modifications have

been made to the Corpus Christi Bay system. More important to this study is the construction of artificial canals. Artificial canals are often used to displace inland floodwaters to the ocean (Tourment et al., 2016). Thus, the construction and alteration of canals could lead to a higher volume of floodwaters reaching the shelf. In December 2019, the city of Corpus Christi approved the construction of a $40 million canal on North Beach for the purpose of displacing floodwaters (Whitehurst, 2019), thus it is especially urgent to understand the history and drivers of shelf hypoxia in this region.

2. METHODS

2.1. Spatial Interpolation of Oxygen Data in the Gulf of Mexico

To better understand the most recent changes in hypoxia, I reconstructed hypoxia contour maps based on previously established bottom water oxygen concentration shapefile data (2001-2019) from the NOAA National Centers for Environmental Information database (May and NOAA Fisheries, 2011; May and NOAA Fisheries, 2016; US DOC, NOAA, and National Marine Fisheries, 2017; US DOC, NOAA and National Marine Fisheries, 2018; NOAA National Marine Fisheries Service, 2019; May and NOAA Fisheries, 2019). Since the arial extent west of the Mississippi River is the focus of the study, the map was cropped to include only the conductivity, temperature, depth (CTD) stations west of the Mississippi River. The 20 shapefiles, one for each year, were gridded using the Kriging technique in ArcGIS Pro (Esri Inc., 2020). The Kriging technique provides the ability to calculate an unknown value of a location, while accounting for the distance and amount of variation among known values in a known geographic position (Paramasivam and Venkatramanan, 2019). Simple kriging was performed in the Geostatistical Wizard workflow using the normal score transformation. Each model was optimized and smoothed. The resulting contours were defined in 0.5 mg/l O_2 intervals. Each contour vector layer was then exported as a raster. All 20 raster datasets were averaged over the past 20 and 5 years using the Raster calculator tool (Figure 2a and 2b).

2.2. Coring Site and Materials

In May 2019, two 3" diameter piston cores (PC) were collected on the Texas Shelf near Mustang Island (Figure 2c) on an expedition led by Dr. Sean Gulick of the University of Texas. A nearshore core (PC3; 27.67°N 97.05 °W; 14 m water depth) of 3.27 m length and an offshore

core (PC2; 27.55° N 96.97° W; 74 m water depth) of 4.28 m length were collected on the R/V Brooks McCall using the TDI-Brooks Piston Coring system. The offshore and nearshore sediments were predominantly siliceous silts and mud interbedded with sandy layers. The expedition metadata states that the nearshore core was flipped to reseal the core, and sediment may have shifted to top of the core. Thus, the surface layer of the core may have been mixed.

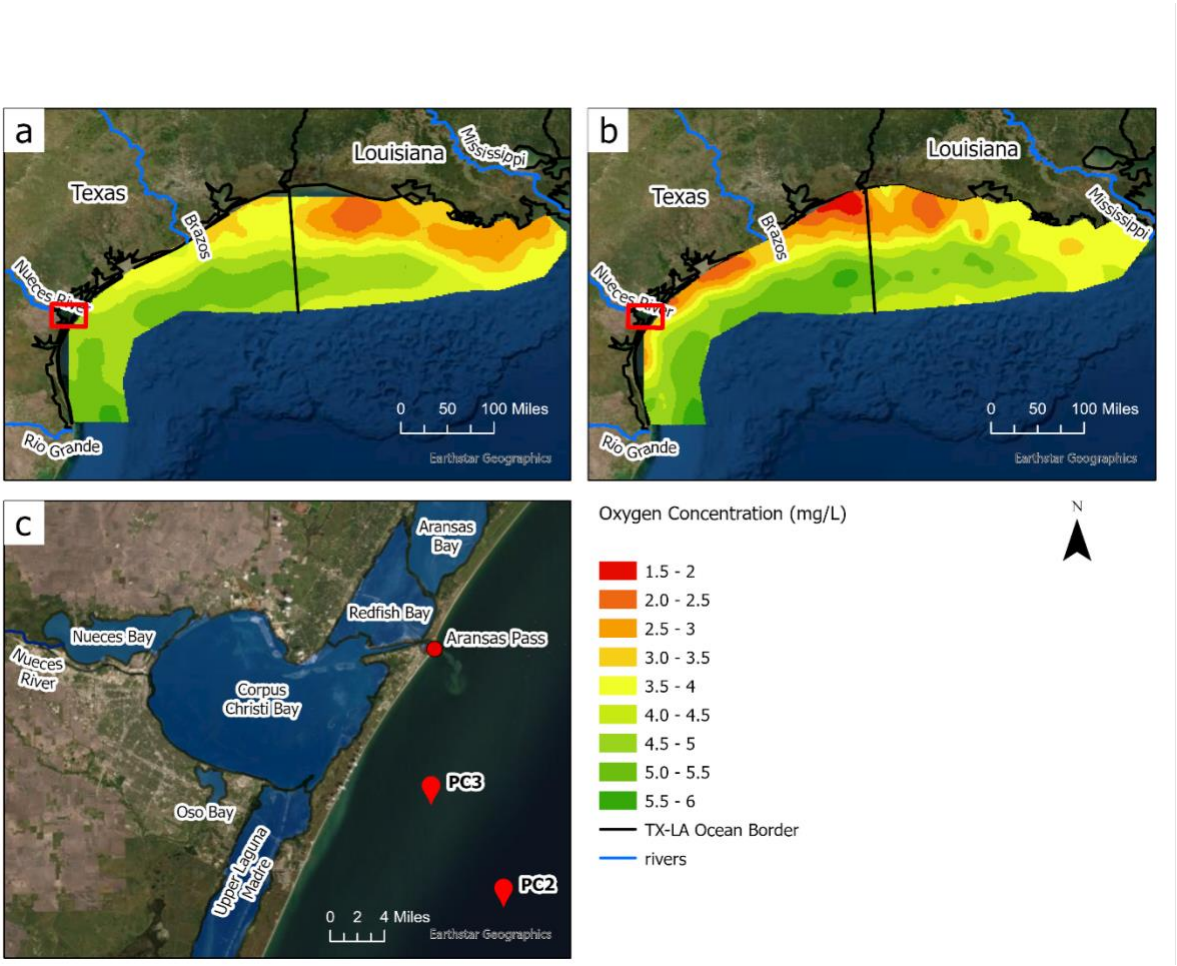

Figure 3: Location of study site and oxygen concentrations in the Gulf of Mexico. (a) 20-year average of bottom-water dissolved oxygen on the Texas and Louisiana shelf from 2001-2019. (b) 5-year average of bottom-water dissolved oxygen on the Texas and Louisiana shelf from 2015-2019. (c) Map of study location: core locations are denoted with

red markers and Aransas Pass is denoted as a solid red circle. Map was made using ArcGIS Pro (Esri Inc., 2020). Dissolved oxygen data was obtained from the NOAA National Centers for Environmental Information database (May and NOAA Fisheries, 2011; May and NOAA Fisheries, 2016; US DOC, NOAA, and National Marine Fisheries, 2017; US DOC, NOAA and National Marine Fisheries, 2018; NOAA National Marine Fisheries Service, 2019; May and NOAA Fisheries, 2019). Base map from Esri et al. (2021).

Approximately 20 cc samples were collected from the nearshore and offshore cores, which yielded a total of 47 samples (18 nearshore samples and 29 offshore samples). Samples were taken at an ~5 cm interval but were adjusted when needed to avoid sand layers that were unlikely to contain foraminifera. Of the 47 samples collected, 14 were used for faunal analyses and ^{210}Pb analysis, 27 were used only for faunal analyses, and 6 were used only for ^{210}Pb analysis. All 47 samples were freeze-dried and weighed for the dry weight (W_{Tot}). Each sample was then disaggregated in deionized (DI) water and wet sieved over a 63 μm sieve. The dried sediment > 63 μm of all samples were weighed (W_{Sand}) and stored in vials. For the ^{210}Pb samples, the dried sediment in the < 63 μm size fraction (mud content) was ground with a mortar and pestle and used for ^{210}Pb analyses, whereas the mud content of the faunal samples was reserved in sampling bags.

The W_{Sand} value was subtracted from the W_{Tot} to obtain the weight of sediment < 63 μm (W_{Mud}) and calculate the percent mud of each sample (W_{Mud} divided by W_{Tot}). The mud percentage in the nearshore samples ranged from 32 to 86%, and the offshore samples ranged from 49 to 99%.

2.3. ^{210}Pb Analysis

The ^{210}Pb activities of the sediments were measured using the ^{210}Po method (Nittrouer et al., 1979; Santschi et al., 2001). The ground mud content of the 20 ^{210}Pb samples was used to minimize the influence of changes in surface area on activity. Approximately 0.5 to 1.0 g of dried sediment was spiked using a ^{209}Po tracer and digested in HCl, HNO_3, and HF. The fractions of ^{210}Po and ^{209}Po were separated and deposited on Ag planchetts (Santschi et al., 2001). The ^{210}Po activity was quantified by α-spectroscopy using Canberra surface barrier detector at Texas A&M University Galveston (TAMUG) at the Coastal Marine Geology Laboratory. ^{210}Pb and ^{210}Po are in secular equilibrium, thus activities are equivalent. The supported ^{210}Pb was subtracted from total ^{210}Pb to obtain excess ^{210}Pb activities ($^{210}Pb_{xs}$). Sediment accumulation rates (SARs) were obtained by calculating a regression line for a segment of the core consistent with steady-state deposition (Equation 3), which was used to calculate the age of each sample (Equation 4). Downcore calculations of age assume a constant SAR and uniform initial ^{210}Pb concentration.

$$SAR = \frac{z\lambda}{\ln (A_d - A_o)} \quad (3)$$

where z = change of depth in regression (cm), λ = radioisotope decay constant (^{210}Pb, 0.031 yr^{-1}), A_d = ^{210}Pb activity at end of regression (dpm g^{-1}), and A_o = ^{210}Pb activity at beginning of regression (dpm g^{-1}). Age of the sediment (t) is equivalent to depth (z) divided by the sediment accumulation rate (SAR).

$$t = \frac{z}{SAR} \quad (4)$$

The 95% confidence intervals (CI) on the age estimates were calculated using the standard error associated with the best fit regression through excess activities with depth.

2.4. Foraminiferal Proxies for Hypoxia

The >63 μm size fraction of the 41 faunal samples used for faunal analyses was split using a micro-splitter until approximately 200 benthic foraminifera were retained (Appendix A). Of the 41 samples selected, 27 were from the offshore core and 14 were from the nearshore core. Benthic foraminifera were then picked from the >125 μm size fraction. I then counted the total number of benthic foraminiferal fossils in each sample and identified each specimen to species using Phleger and Parker (1951) and Poag (2015).

After foraminiferal identification, individuals belonging to the *Ammonia* and *Elphidium* genera were counted in each sample. These two values were then used in the A-E index equation (Equation 1). As for the PEB index, the abundances of *Pseudononion atlanticum*, *Epistominella vitrea*, and *Buliminella morgani* were used in the PEB index equation (Equation 2; Figure 3). The method for the PEB index was then modified (PEBn), grouping the counts of *Nonionella opima* (a morphologically similar taxon to *Pseudononion atlanticum)* to the value of N_P (Tichenor et al., 2016; Figure 3). To determine whether *E.vitrea* dominates the PEBn signal, the percent abundance of *E. vitrea* relative to the PEBn taxa was calculated.

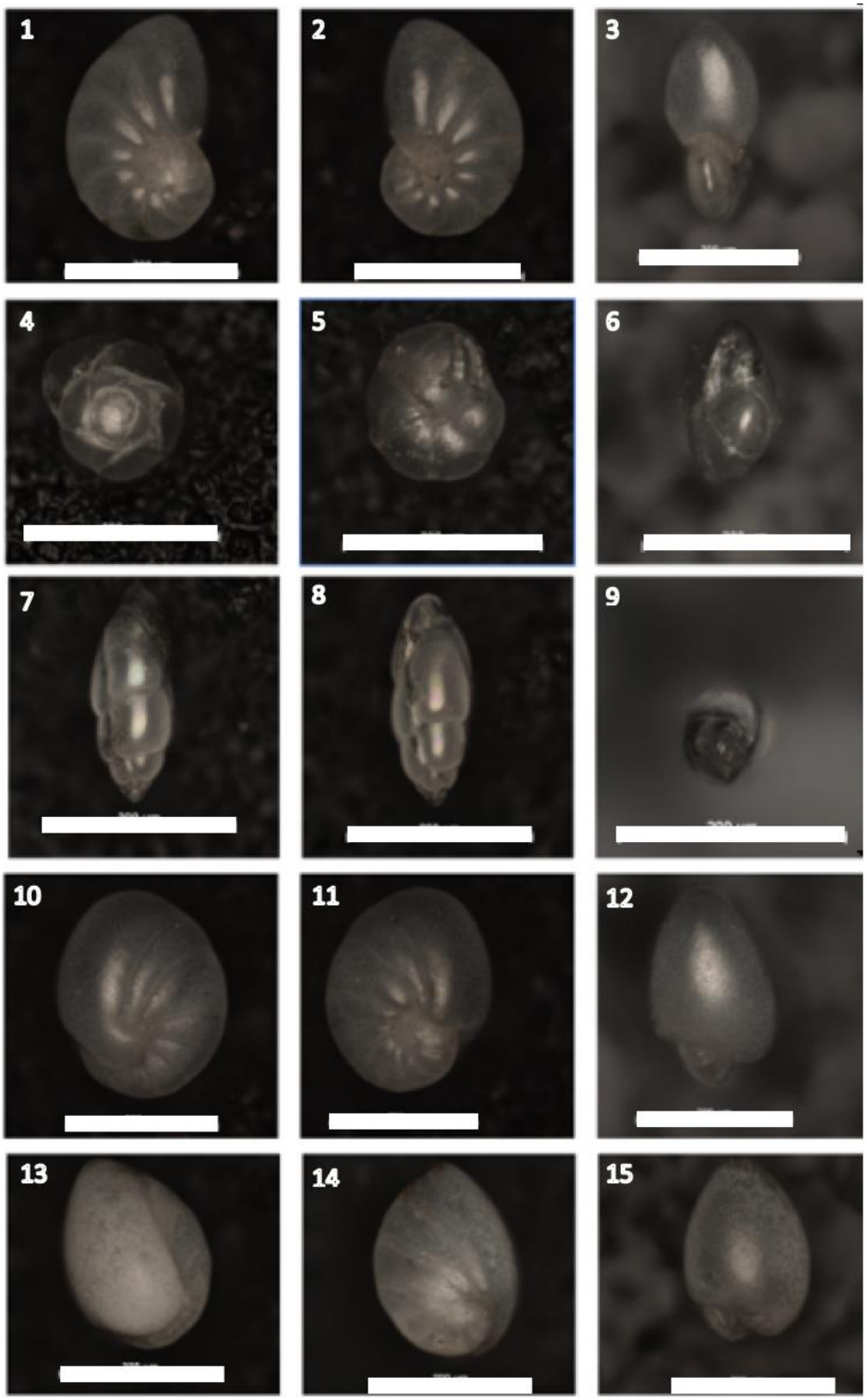
1
2
3
4
5
6
7
8
9
10
11
12
13
14
15

Figure 4: Photomicrographs of PEB (1-9) and PEBn (1-15) index taxa. Scale bars are 200 µm. *Pseudononion atlanticum* (1-3): 1- spiral side, 2 - umbilical side, 3 – aperture (Cushman, 1947); *Epistominella vitrea* (4-6): 4 - spiral side, 5 - umbilical side, 6 – aperture (Phleger, 1953); *Buliminella morgani* (7-9): 9 – aperture (Anderson, 1961); *Nonionella opima* morphotype 1 (10-12): 10- umbilical side, 11 – spiral side, 12 – umbilical flap (Cushman, 1947); *Nonionella opima* morphotype 2 (13-15): 13- umbilical side, 14 – spiral side, 15 – umbilical flap (Cushman, 1947).

2.5. Ecological Metrics

To test whether a decline in diversity is linked to hypoxia, richness and evenness was calculated on all assemblages at the genus-level. The genus level was preferred because of uncertainties in taxonomic grouping at the species-level for some genera. Taxonomic richness was calculated as the number of genera after rarefying to one less the number of individuals in the smallest sample; this technique accounts for sample-size effects on richness (Sanders, 1968). Evenness was calculated as the probability of interspecific encounter (PIE). This method is insensitive to differences in sample size (Hurlbert, 1971). PIE was calculated using the paleoTree (function “HurlbertPIE”; Bapst et al., 2012) and rarefaction was calculated using the vegan package (function “rarefy”; Oksanen et al., 2015) in the R programming language (R Core Team, 2021).

2.6. PCO Analysis

I performed multivariate ordination on the proportional abundance of the foraminiferal faunas in samples from both cores in a single analysis to summarize downcore faunal variation and its relationship to past environmental conditions. A principal coordinate analysis (PCO) was most appropriate for this study due its ability to analyze a Bray-Curtis dissimilarity matrix, which is the most ecologically appropriate (Legendre and Legendre, 2003). The PCO analysis was conducted on the proportional abundances of taxa at the genus-level dataset using the vegan package (functions “decostand”, “vegdist”, “cmdscale” and “wascores”; Oksanen et al., 2015) of the R programming language (R Core Team, 2021). I determined the number of axes to interpret based on the proportion of the total variation that each component explains (the eigen value of the component of interest divided by the sum of all eigen values). I then tested the hypothesis that the PCO scores reflect changes in salinity and oxygenation by comparing the ordination scores of taxa with the known environmental preferences of the genera in the modern. To determine whether PCO axis scores are an indicator of oxygenation, I performed Spearman rho correlation tests between the PCO axis scores and each foraminiferal index (PEB, PEBn and A-E index) using the ‘cor.test’ function in the R base package, ‘stats’, in the R programming language (R Core Team, 2021). Sample scores in ordination spaces were compared between the two sites to determine whether the nearshore or offshore samples clustered in ordination space. To test whether the PCO axis scores of each site occupy different portions of ordination space, I performed a Mann-Whitney U test using the ‘wilcox.test’ function in the R base package, ‘stats’, in the R programming language (R Core Team, 2021).

2.7. Time Series Analyses

To determine the tempo and mode of temporal changes in the richness, evenness, PEB, PEBn and A-E trends, I used maximum likelihood model selection methods to test for data fit to four models of downcore change: URW (unbiased random walk), GRW (general random walk), stasis, and a temporal shift that separates periods of stasis. If the URW model is supported, then there is no discernable pattern to the data; each successive sample is independent from one another. If GRW is supported, then there is a supported trend in time – data continually increases or decrease over time. Stasis will fit the best if the data varies around a single value through time. If the shift model is supported, then a period of status will be abruptly interrupted by a shift to a new static value. These models test whether there is a gradual change or an abrupt shift in the ecological metrics with depth in each core.

Each model was constrained to having a minimum segment length of 2 samples, allowing testing of a shift with as few as 2 samples in the time series segment before or after the shift. All models were compared using the Akaike Information Criterion (AIC), with lower values indicating a better supported model. The AIC scores of each model were standardized by calculating the AIC weights of each model, which measure the amount of support relative all models tested for a given dataset. I followed the procedure by Hunt et al. 2006 and using the PaleoTS package (Hunt, 2019) in the R programming language (R Core Team, 2021).

2.8. Stable Isotope Analysis

Stable isotope analyses were performed on *Elphidium excavatum*, a robust foraminifer common in both cores. Five samples were analyzed in the nearshore core and 23 were analyzed in the offshore core. From each sample, approximately 90 -105 μg of carbonate was picked.

More individuals were picked for samples with smaller *E. excavatum*; thus, the number of individuals picked among all samples ranged from 5 to 90. Before analyses, *E. excavatum* was ultrasonicated in 10% methanol solution to remove internal contaminants, washed in DI water, and reweighed to ensure ~90 -105 μg were retained. Additional individuals were processed if foraminiferal carbonate was less than 90 μg for a given sample after cleaning. Samples were digested in 105% H_3PO_4 (specific gravity = 1.92-1.93 g/mL) at ~70 °C on a Thermo Finnigan Kiel IV automated carbonate device. The CO_2 product was then analyzed on a Thermo Finnigan MAT 253 isotope ratio mass spectrometer at Texas A&M University (TAMU) Stable Isotope Geosciences Facility (SIGF) in the College of Geosciences. The $\delta^{18}O$ and $\delta^{13}C$ values were then calibrated against International Atomic Energy Agency (IAEA) 603 ($\delta^{13}C$ = 2.46‰ and $\delta^{18}O$ = -2.37‰) and NBS-19 carbonate standard ($\delta^{18}O$ = -2.20‰ and $\delta^{13}C$ = 1.95‰). All delta values are on the VPDB scale and precisions are 0.04‰ for $\delta^{13}C$ and 0.06‰ for $\delta^{18}O$ based on the 6 replicates of a laboratory standard used in every run. *E. excavatum* is an infaunal foraminifer, thus $\delta^{13}C$ values may reflect changes in the sediment pore waters.

The $\delta^{18}O$ composition of foraminiferal tests are primarily influenced by the temperature of calcification, the $\delta^{18}O$ of the ambient water, and vital effects. In this study, I assume that temperature remains relatively constant through time and does not differ between sites. Past studies suggest that *E. excavatum* may be prone to vital effects (disequilibria due to metabolic processes) that would affect the measured foraminiferal $\delta^{18}O$ values. *E. excavatum* could experience $\delta^{18}O$ enrichment relative to calcite equilibrium of 1.0 to 1.5‰ (Bauch et al., 2004) or depletion of ~ 1.0‰ (McCorkle et al., 1997). Thus, foraminiferal $\delta^{18}O$ values may be offset due to the vital effects that *E. excavatum* may experience, causing *E. excavatum* to not be in equilibrium with the $\delta^{18}O$ of the seawater. Lastly, the $\delta^{13}C$ of *E. excavatum* may be prone to vital

effects that vary with changes in salinity near estuarine regions, where lower salinities were associated with lower $\delta^{13}C$ values (Polyak et al., 2003).

Following the methods by Strauss et al. (2012), I calculated the salinity change associated with $\delta^{18}O$ change during the Nueces River flooding in 2002. I derived two-component mixing model equations from known salinity and $\delta^{18}O$ values of: (1) the Nueces River ($\delta^{18}O$ of -2.8‰ and salinity of 0 psu; Dutton et al., 2005) and GoM ($\delta^{18}O$ of 1.1‰ and salinity of 36 psu; Strauss et al., 2012), and the (2) Mississippi/Atchafalaya River ($\delta^{18}O$ of -5.8‰ and salinity of 0 psu; Lee and Veizer, 2003; Strauss et al., 2012) and GoM ($\delta^{18}O$ of 1.1‰ and salinity of 36 psu; Strauss et al., 2012). I assume that the Mississippi/Atchafalaya waters are 70% Mississippi flow and 30% Atchafalaya flow (determined by the Old River Control Structure and was done by Strauss et al., 2012), which average a $\delta^{18}O$ of -5.8‰ (Lee and Veizer, 2003).

3. RESULTS

3.1. Recent Hypoxia in Instrumental Records

In the 20-year average, the Texas Shelf did not have any area with oxygen concentrations < 3 mg/L. However, the 5-year average shows that the Texas Shelf up 10,253.4 km^2 of area < 3 mg/L, or 37% of area west of the Mississippi that is < 3 mg/L. I encourage caution in interpreting these maps, though, because the temporal and spatial resolution of the CTD stations are not consistent among years and sampling biases may influence the contour maps.

3.2. $^{210}Pb_{xs}$ Analysis and Core Age Models

The downcore profiles of the offshore and nearshore cores are shown in Figure 5. The ^{210}Pb values do not change in the upper 8 cm of the offshore core and were excluded from calculation of the SAR. The $^{210}Pb_{xs}$ activity never reached a stable level in the deeper portion of the core, thus background levels of ^{210}Pb were not obtained. The SAR of ~ 2.5 cm/y (CI: 1.82 to 3.09 cm/yr) of the offshore core was determined from the $^{210}Pb_{xs}$ data from 8 cm to 49 cm (n=9; Figure 5a). The age of the sediment from 0 to 49 cm had a maximum age of 20 years or ~2000 CE (CI: 1992-2003 CE). Under the assumption of constant SAR, the oldest sample in the offshore core would be 170 years or ~1850 CE (CI: 1789-1883 CE).

The $^{210}Pb_{xs}$ activities in the upper 8 cm of the nearshore core do not change and were excluded from calculation of the SARs (Figure 5). The $^{210}Pb_{xs}$ activity never reached a stable level in the deeper portion of the cores, thus background levels of $^{210}Pb_{xs}$ were not obtained. Two SARs of the nearshore core were determined from the excess $^{210}Pb_{xs}$ below 8 cm, due to portions of the core having slightly different slopes (Figure 4b). The 10 to 25 cm depth of the nearshore

core generated a SAR of ~0.50 cm/y (.30 to .69 cm/yr) and the 26 to 43 cm depth generated a SAR of ~0.56 cm/y (.44 to .73 cm/yr). The SAR representing the upper portion (3 cm to 23 cm) of the evaluated core represent as maximum age of ~ 45 years or ~1970 CE (CI: 1943-1986 CE). The SAR representing the lower portion (24 cm to 41 cm) of the evaluated core represents a maximum age of ~70 years or ~1950 CE (CI: 1925-1963 CE). To extrapolate to portions of the core for which there are no $^{210}Pb_{xs}$ data, I use the SAR from the lower portion of the core; this gives the lowermost sample in this nearshore core an estimated age of ~550 years or ~1470 CE (1284-1580 CE).

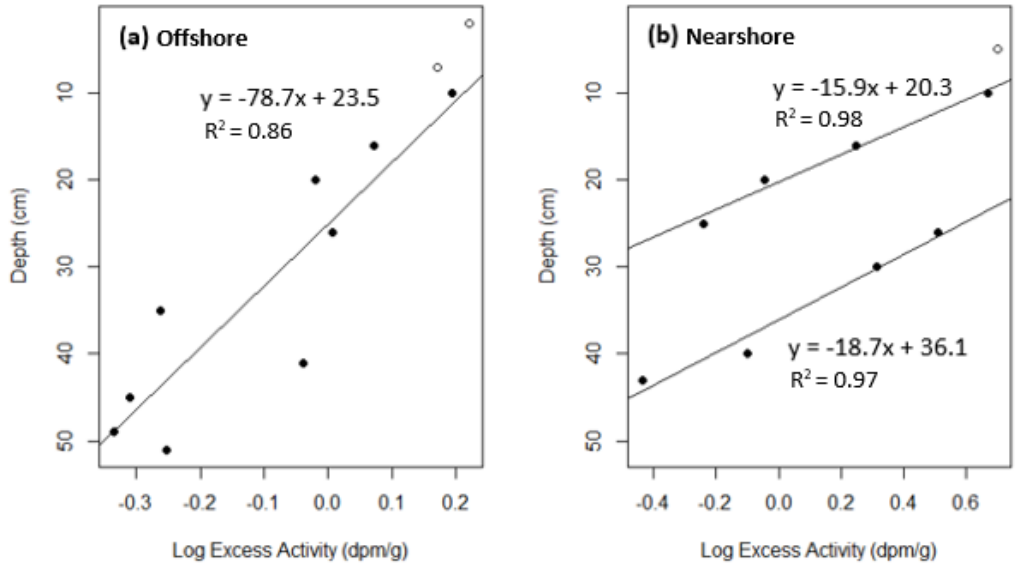

Figure 5: Excess ^{210}Pb activity measured in Texas cores. The lines represent sediment accumulation rate (SAR) determined using the excess ^{210}Pb activity below the layer of mixed depth (0-8 cm) for both the offshore core (a) and nearshore core (b). Solid circles were the samples used to calculate the SARs. Open circles are samples within the mixed depth layer.

3.3. Faunal Indices for Hypoxia

All the taxa used to calculate the PEB, PEBn and A-E index were present and abundant in both nearshore and offshore cores. The PEB index in the majority of offshore and nearshore samples were not dominated by *E. vitrea*. In the offshore core, *E. vitrea* was present in all the samples except one. In all the offshore samples, the mean percent abundance of *E. vitrea* relative to the PEB taxa was 34 % (standard deviation (sd) = 24.1). In the nearshore core, only one sample contained *E. vitrea* in which it accounted for only ~ 6% of the PEB taxa present. Thus, *E. vitrea* was more abundant in the offshore site than the nearshore site.

N. opima also does not dominate the PEBn index values in the offshore or nearshore samples. In all the offshore samples, the percent abundance of *N. opima* relative to the abundance of PEBn taxa (P_n), averaged 26% (sd = 20.2), whereas the percent abundance of *P. atlantica*, relative to the abundance of PEBn taxa (P_P) averaged (sd = 29.0). In the nearshore samples, the mean value of P_n was 45% (sd = 32.1) and the mean P_P value was 46% (sd= 30.0).

3.3.1. PEB and PEBn

In the offshore core, the PEB and PEBn indices have similar temporal patterns and do not deviate from one another (Figure 6a). PEB and PEBn values are over 7% in the majority of offshore samples (PEB > 7%: 19 of 27 samples; PEBn > 7%: 22 of 27 samples) with mean PEB and PEBn indices of 9.7% (sd = 5.0) and 13.5% (sd = 7.3), respectively. PEBn values remained lower than the overall mean of the time series after ~127 cm, and the majority of the PEBn values remain above the mean after 127 cm (9 of 16 samples). The PEB and PEBn values of the most recent sample (0-2 cm; PEB: 18%; PEBn: 25%), were ~2x greater than the core's mean PEB and PEBn values.

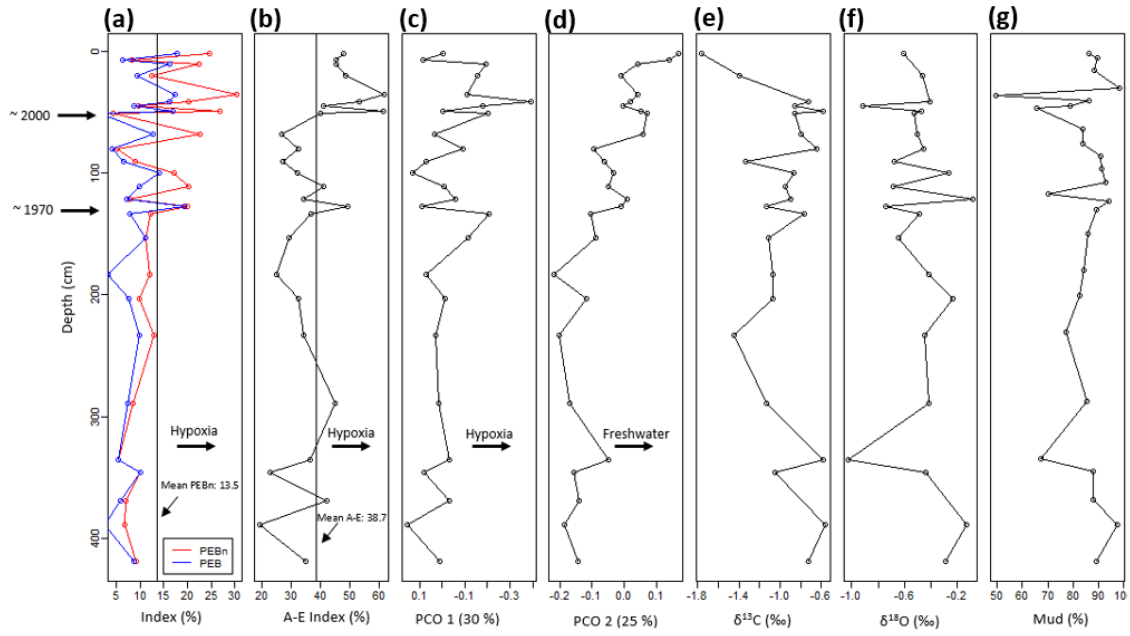

Figure 6: Variables with depth in the offshore core (PC2). (a) PEB and PEBn indices; (b) A-E index; (c) PCO 1 axis scores; (d) PCO 2 axis scores; (e) $\delta^{13}C$ values of *E. excavatum*; (f) $\delta^{18}O$ values of *E. excavatum;* (g) Percent of mud (< 63µm). Solid black vertical lines in a-b represent mean values of the specified index. Black arrows on y-axis represent important estimated ages mentioned in the text. Black arrows in the body of the plot represent environment interpretation of the proxy. Confidence intervals for 2000 CE: 1992 CE to 2003 CE. Confidence intervals for 1970 CE: 1950 to 1979 CE.

In the nearshore core, the PEB and PEBn have similar trends and do not deviate from each other until 50 cm (Figure 7a). At ~43 cm, the percent abundance of *N. opima* increases dramatically causing the PEBn value to increase above the PEB value. PEB and PEBn values generally remain under 7% throughout the core (PEB < 7%: 12 of 14 samples; PEBn < 7%: 11 of 14 samples). The mean PEB of all samples was 3.0 % (sd = ~ 2.5) and the mean PEBn value was 6.5% (sd = 5.0). PEBn values generally remain below the mean value, except for 6 samples; notably, at 43 cm the PEBn value was ~3x the mean.

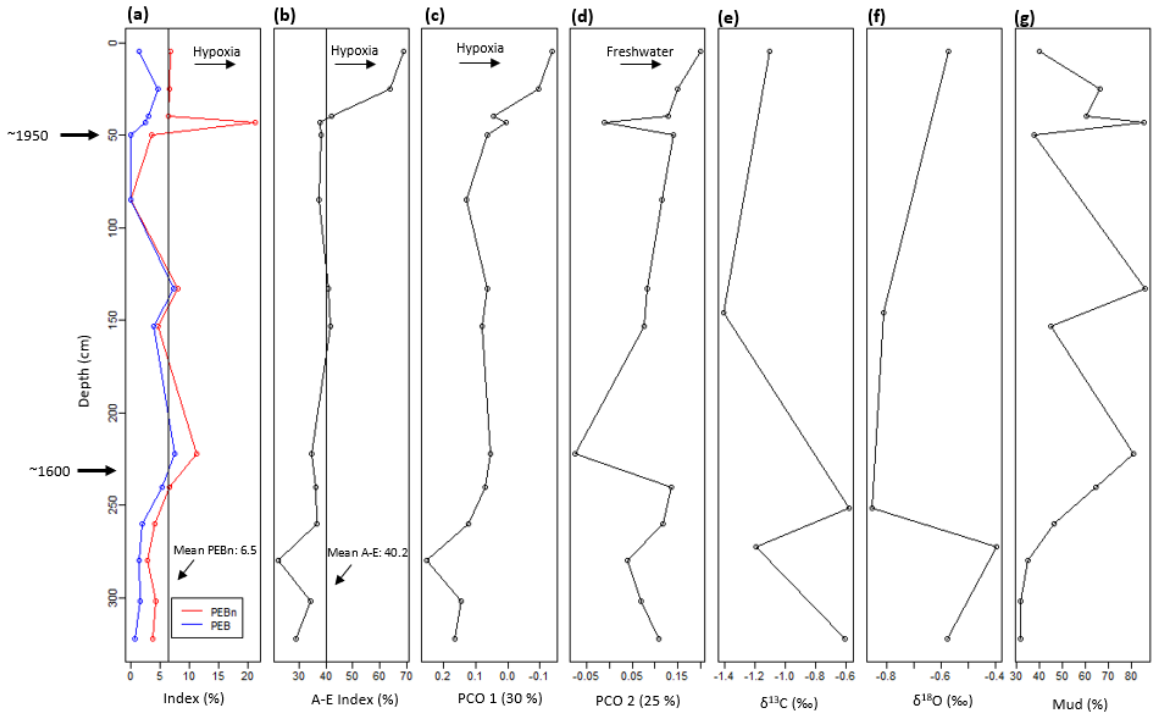

Figure 7: Variables with depth in the nearshore core (PC3). (a) PEB and PEBn indices; (b) A-E index; (c) PCO 1 axis scores; (d) PCO 2 axis scores; (e) δ^{13}C values of *E. excavatum*; (f) δ^{18}O values of *E. excavatum;* (g) Percent of mud (< 63µm). Solid black vertical lines in a-b represent mean value of the specified index. Black arrows on y-axis represent important

ages mentioned in the text. Confidence intervals for 1950 CE: 1925 CE to 1963 CE. Confidence intervals for 1600 CE: 1460 to 1685 CE.

On average, the offshore core generated higher PEB and PEBn values relative to the nearshore core. The mean PEB and PEBn values of the offshore core was ~3x and ~2x higher, respectively, than the nearshore mean values.

3.3.2. A-E

In the offshore core, A-E values remain above the mean value of 38.7% (sd: 10.9) after 51 cm, whereas below 51 cm only 4 samples rise above the mean. Samples below 51 cm had a mean A-E value of 33% (sd: 7.8).

In the nearshore core, A-E values had a mean of 35% from 322 cm to 43 cm to 322 cm (n=11; sd = 5.8; Figure 7b). From 43 cm to the most recent sample (3 cm), the mean A-E value was 50% (n=5; sd = 15.1). The highest A-E value occurred in the most recent sample (A-E: 69%).

The offshore core had a higher mean A-E than the nearshore core. Moreover, higher A-E values occurred in the offshore core than in the nearshore core (maximum A-E of 69% and 62%, respectively).

3.4. Faunal Composition

Foraminifera were present in every sample of the offshore and nearshore cores, with no barren samples. Samples from the offshore core (n=27), PC2, contained 33 genera. Fourteen samples from the nearshore core, PC3, contained 25 genera. Other than the PEB and A-E taxa, *Hanzawai concentrica* was the most abundant taxon in the offshore and nearshore samples

(Appendix A). Overall, richness was higher in the offshore core than in the nearshore core (Figure 8). Richness values ranged from 8.28 to 16.89 genera (mean = 11.04; sd = 5.10) in the offshore core and 0.12 to 14.74 genera (mean = 7.26; sd = 5.10) in the nearshore core. Similarly, evenness was higher in the offshore core than the nearshore core. Evenness in the offshore core ranged from 0.64 to 0.92 (mean = .82; sd=0.06) and in the nearshore core evenness ranged from 0.66 to 0.88 (mean = .73; sd=0.06). Richness and evenness are lowest from 3 cm to 25 cm of the offshore core and evenness is low from 0 cm to 7 cm of the nearshore core (Figure 8).

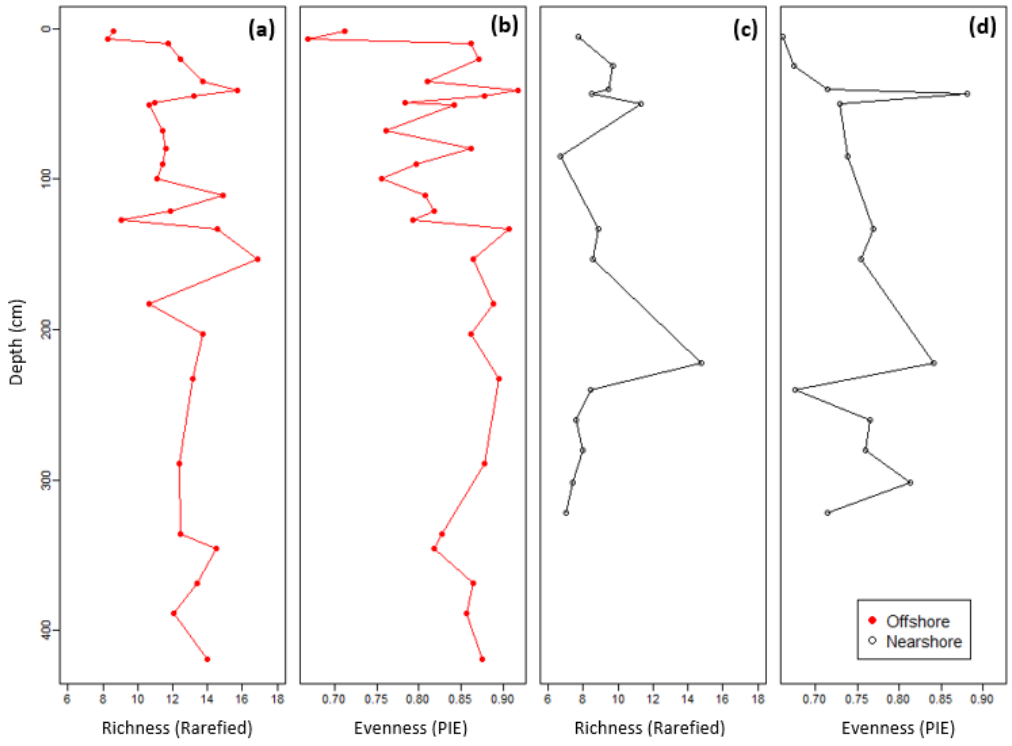

Figure 8: Evenness (PIE) and richness (rarefied) downcore. Genus-level data with depth of the offshore core (a-b) and nearshore core (c-d).

PCO axis 1 explains 30% of the total faunal variance. Nearshore sample have more positive scores, whereas most of the offshore sites have negative PCO axis 1 scores (Figure 7a). Statistically, the nearshore and offshore sites occupy different parts of the PCO axis 1 (Mann-

Whitney U= 95; $p < 0.01$). PCO axis 2 explains 25% of the variance. Most of the nearshore samples (13 of 16) have positive PCO axis 2 scores, whereas most of the offshore samples have negative scores (18 of 27). Both sites statistically occupy different portions of the PCO 2 axis (Mann-Whitney U = 54; $p < 0.001$).

On PCO axis 1, all miliolids (*Triloculina, Quinqueloculina, Milliamina, Sigmoilina, and Pygro*) have positive scores, and low-oxygen taxa (*Ammonia, Buliminella, Bulimina, Brizalina, Cassidulina, Epistominella, Fursenkonia, Nonionella, Pseudononion, and Buliminella)* have negative values (Figure 7b; oxygen tolerances from Murray, 2006). All the PEBn taxa (*Pseudononion, Epistominella, Buliminella,* and *Nonionella*) have negative PCO axis 1 scores, and *Ammonia* from the A-E index generated a more negative value than *Elphidium*. The PCO 1 axis scores correlate with all foraminiferal indices: PEB index values (r_s= -0.34; p-value= < 0.05), PEBn index values (r_s= -0.37; p-value= < 0.05) and the A-E index values (r_s= -0.49; p-value= < 0.005). On PCO axis 2, the most positive values are associated with two rare, agglutinated taxa, *Cribrostomoides* and *Karreriella*. *Ammonia* and *Elphidium* have positive PCO axis 2 scores (Figure7b), whereas the PEB taxa have all negative PCO axis 2 scores. *N. opima*, the taxon that defines the PEBn index, had a positive value.

In the offshore core, PCO axis 1 scores increase from 100 cm core depth until 5 cm (Figure 6c). The PCO axis 2 scores in this core gradually increase from 180 cm to the core top (Figure 6d). In the nearshore core, PCO axis 1 scores increase from 50 cm until the core top (Figure 7c), and the PCO axis 2 scores gradually increase from 153 cm to the core top (Figure 7d).

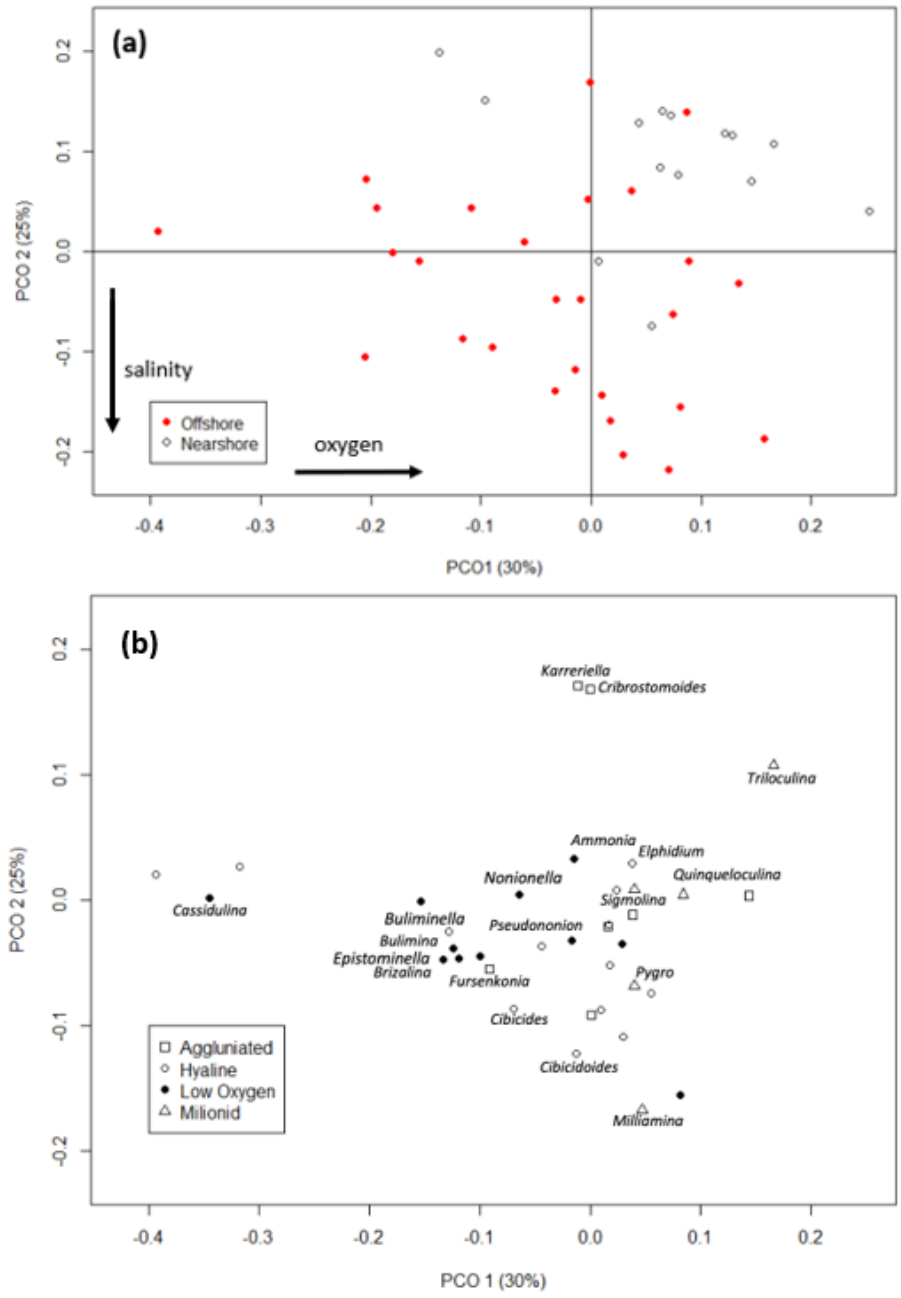

Figure 9: PCO axis scores 1 and 2 of species and sites. (a) Site scores in the nearshore core (open circles) and offshore core (red circles). (b) PCO axis scores 1 and 2 of the genera. Taxa are annotated by symbols based on the ecology of the genus. All taxa designated as low-oxygen are hyaline.

3.5. Time-Series Analyses

In the offshore core, stepped changes with depth occurred in all ecological metrics (PEB, PEBn, A-E, richness, and evenness). Among the offshore foraminiferal assemblages, PEB had one statistically supported step-change (an increase at 51 cm; Table 1), since the one-shift model (AICc wt = 0.79) was better supported than the stasis model (AICc wt = 0.21), and the other models had no support. Similarly, PEBn had one statistically supported step-change (an increase at 51 cm; AICc wt = 0.85; Table 2); the AICc weight for the stasis model was lower (AICc wt = 0.15) and the other models had no support. The A-E index had one statistically supported step (increase at 51 cm; AICc weight = 0.99; Table 2), which was better supported than the stasis model (AICc wt = 0.01); the other models had no support. Thus, all three foraminiferal oxygen indices had one statistically supported step – an increase in the index value at 51 cm. Under the current age model and the assumption of constant sedimentation rates, 51 cm is ~2000 CE (CI: 1992-2003 CE).

For offshore richness, the one-step model (AICc wt = 0.74; decrease at 10 cm) was better supported than the stasis (AICc wt = 0.26), URW (AICc wt = 0.00), and GRW (AICc wt = 0.00) models. Similarly, the one-shift model for offshore evenness (AICc wt = 0.79; decrease at 10 cm) was better supported than the stasis (AICc wt = 0.21), URW (AICc wt = 0.00), and GRW (AICc wt = 0.00) models. Both richness and evenness in the offshore core had one statistically supported step represented by a decrease in value at 10 cm, or ~2016 CE (CI: 2015-2016 CE) as suggested by the current age model and the assumption of constant sedimentation rates.

In the nearshore core, stepped change occurred in both the PEB and PEBn indices, represented by an increase in index value at 240 cm, or ~1600 CE (CI: 1471-1691 CE) under the current age model and the assumption of constant sedimentation rates. The one-shift model was

the best supported model for PEB and PEBn (AICc wt = 1.00) and all other models received no weight; in both cases the shift occurred at 240 m (Table 2). The temporal pattern of the A-E index was most similar to stepped change at 40 cm (AICc wt = 0.54) and the GRW model was the second-best supported model (AICc wt = 0.34). This shift occurred at ~1950 CE (CI: 1925-1963 CE), under the current age model and the assumption of constant sedimentation rates. For both richness or evenness in the nearshore core, stasis was the best supported model for both metrics (AICc wt = 0.76 and 0.74, respectively), and was better supported than the URW (AICc wt = 0.11 and 0.00, respectively), GRW (AICc wt = 0.02 and 0.00, respectively), and one-shift (AICc wt = 0.11 and 0.26, respectively) models.

Table 1: Time series model selection of hypoxia indices and ecological metrics. AICc values and Akaike weights based on AICc values for five time-series models of changes in species richness, PIE, and hypoxia indices (PEB, PEBn and AE): URW (unbiased random walk), GRW (general random walk), stasis, and 1-Shift; n represents the number of samples in each model. Shift start indicates the core depth and age of the oldest sample prior to the shift. Shaded rows represent best supported model. PC2 = offshore core and PC3 = nearshore core.

Model	AICc	AICc wts	shift start (cm)
PC2 - PIE (n=27)			
GRW	-52.98	0.00	NA
URW	-55.36	0.00	NA
Stasis	-72.88	0.21	NA
1-Shift	-75.28	0.79	10
PC2 - Richness (n=27)			
GRW	131.48	0.00	NA
URW	129.14	0.00	NA
Stasis	117.23	0.26	NA

1-Shift	115.15	0.74	10
PC2 - PEB (n=27)			
GRW	220.70	0.00	NA
URW	203.18	0.00	NA
Stasis	167.18	0.21	NA
1-Shift	164.57	0.79	51
PC2 - PEBn (n=27)			
GRW	225.58	0.00	NA
URW	223.07	0.00	NA
Stasis	187.28	0.15	NA
1-Shift	183.76	0.85	51
PC2- AE (n=27)			
GRW	222.76	0.00	NA
URW	220.24	0.00	NA
Stasis	208.72	0.01	NA
1-Shift	198.29	0.99	51
PC3 - PIE (n=14)			
GRW	-10.72	0.00	NA
URW	-14.02	0.00	NA
Stasis	-33.40	0.74	NA
1-Shift	-31.26	0.26	NA
PC3 - Richness (n=14)			
GRW	70.21	0.02	NA
URW	66.92	0.11	NA
Stasis	63.11	0.76	NA
1-Shift	66.96	0.11	NA
PC3 - PEB (n=14)			
GRW	111.81	0.00	NA
URW	108.51	0.00	NA
Stasis	88.92	0.00	NA
1-Shift	73.95	1.00	240
PC3 - PEBn (n=14)			
GRW	111.73	0.00	NA
URW	108.42	0.00	NA
Stasis	88.84	0.00	NA
1-Shift	74.00	1.00	240
PC3- AE (n=14)			
GRW	100.71	0.12	NA
URW	98.56	0.34	NA
Stasis	114.08	0.00	NA
1-Shift	97.64	0.54	40

3.6. Stable Isotope Analysis

The oxygen isotopes values of the offshore core ranged from -1.0‰ to -0.1‰, whereas the nearshore core ranged from -0.9‰ to -0.4‰. Carbon isotopes values of the offshore core ranged from -1.8‰ to -0.6‰ and the nearshore core ranged from -1.4‰ to -0.6‰. There was no significant correlation between $\delta^{18}O$ and $\delta^{13}C$ of *E. excavatum o*f the offshore core (r_s= 0.11; p-value = 0.63) or nearshore core (r_s= -0.18; p-value = 0.77; Figure 8).

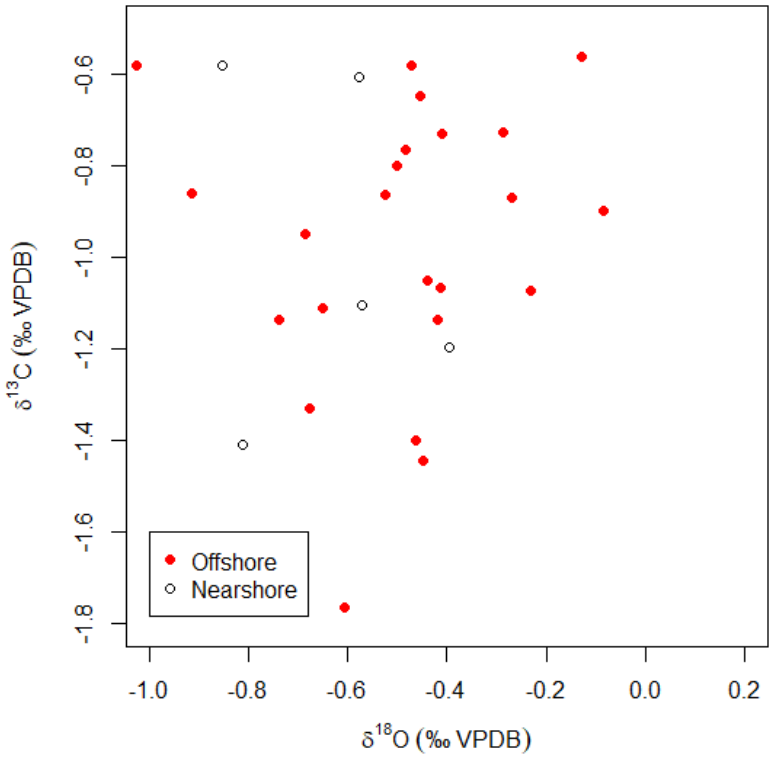

Figure 10: Scatterplot of the isotope values of *E. excavatum* of the nearshore core (PC3) and offshore core (PC2).

In the offshore core, $\delta^{18}O$ decreased from -0.47‰ to -0.91‰ at 49 cm, resulting in a -.4‰ decrease. The most recent samples had two of the lowest $\delta^{13}C$ values; -1.76‰ at 2 cm and

-1.4‰ at 20 cm (Figure 7e). There were no significant Spearman rank-order correlations between the stable isotope values and foraminiferal indices (Table 2) or between the stable isotope values and the PCO axis scores (Table 3) in the offshore core.

In the nearshore core, only five samples were analyzed, and no notable changes were seen in $\delta^{18}O$ or $\delta^{13}C$. No significant correlation occurred between the stable isotope values and foraminiferal indices (Table 2) or between the stable isotope values and the PCO axis scores (Table 3).

Table 2: Spearman rho between indices and stable isotopes. Spearman rho correlation coefficient values (r_s) and two-tailed p values (p (2t)) between foraminiferal indices and stable isotope values. Var = variable

Core	Var.1	Var.2	r_s	p (2t)
PC2	PEB	$\delta^{13}C$	-0.25	0.25
PC2	PEBn	$\delta^{13}C$	-0.25	0.25
PC2	A-E	$\delta^{18}O$	-0.33	0.13
PC3	PEB	$\delta^{13}C$	-0.40	0.52
PC3	PEBn	$\delta^{13}C$	-0.60	0.35
PC3	A-E	$\delta^{18}O$	-0.30	0.68

Table 3: Spearman rho between PCO scores and stable isotopes. Spearman rho correlation coefficient values (r_s) and two-tailed p values (p (2t)) between PCO axis scores and stable isotope values. Var = variable.

Core	Var. 1	Var. 2	r_s	p (2t)
PC2	PCO 1	$\delta^{18}O$	0.21	0.35
PC2	PCO 1	$\delta^{13}C$	-0.17	0.42
PC2	PCO 2	$\delta^{18}O$	-0.38	0.08
PC2	PCO 2	$\delta^{13}C$	0.08	0.72

PC2	PCO 3	$\delta^{18}O$	0.30	0.16
PC2	PCO 3	$\delta^{13}C$	0.16	0.47
PC3	PCO 1	$\delta^{18}O$	-0.30	0.68
PC3	PCO 1	$\delta^{13}C$	0.10	0.95
PC3	PCO 2	$\delta^{18}O$	-0.10	0.95
PC3	PCO 2	$\delta^{13}C$	-0.20	0.78
PC3	PCO 3	$\delta^{18}O$	0.30	0.68
PC3	PCO 3	$\delta^{13}C$	0.10	0.95

The associated change in salinity with change in $\delta^{18}O$ was only calculated for the offshore core, since only 5 samples were analyzed in the nearshore core. After assuming a two-component mixing of the Nueces River and GoM, the relationship between $\delta^{18}O$ and salinity was derived:

$$\text{Salinity} = 9.2309\ (\delta^{18}O_{foram}) + 25.846$$

The -0.4‰ change in $\delta^{18}O$ at 49 cm in the offshore core would represent a salinity decrease of 4.2 psu if all the $\delta^{18}O$ change is attributed to variation in input from the Nueces River. Two-component mixing between the Mississippi River and GoM yields the relationship:

$$\text{Salinity} = 5.2174\ (\delta^{18}O_{foram}) + 30.261$$

Using this equation, the -0.4‰ $\delta^{18}O$ shift equates to a decrease in salinity of 2.4 psu, when assuming mixing between the Mississippi- Atchafalaya Rivers and the GoM. Overall, local river discharge from the Nueces River generates larger changes in salinity than the Mississippi River.

4. DISCUSSION

4.1. Recent Evidence for Hypoxia on the Texas Shelf

Spatial averages of instrumental oxygenation data over the last 20 years, suggest that hypoxic conditions on the Texas shelf have become more severe and more widespread in the last 5 years (Figure 1). This increase in hypoxia suggests that either Texas flooding has become more severe over the past 5 years or the Mississippi-Atchafalaya plume is extending onto the Texas shelf more frequently. Brazos River discharge data collected near Rosharon, Texas (USGS River Gage 08116650, http:// waterdata.usgs.gov) supports that two extreme flooding events of the Brazos River have occurred within the past 5 years. These major flooding events occurred in 2019 and 2016 and generated 23,090 ft^3/m and 26,130 ft^3/m of flood waters, respectively. These flooding events generated discharges ~3x larger than Brazos River's average discharge of 8,459.8 ft^3/m (average from 1970 to 2019). The 5-year averaged map shows a separate hypoxic zone occurring east of the Brazos River whereas severe hypoxic conditions are not seen near the Mississippi River, suggesting the two are not contiguous. However, uneven spatial and temporal sampling may bias the results seen in the 5- and 20-year averaged maps, thus the conclusions drawn from my maps are preliminary.

4.2. Viability of Foraminiferal Index Methods on the Texas Shelf

This study considered the various concerns raised by past studies regarding the use of *E. vitrea* as an indicator for hypoxia, which is included in both the PEB and PEBn indices. High abundances of *E. vitrea* along the Louisiana-Texas Shelf have been attributed to environmental factors other than oxygenation (Blackwelder et al., 1996; Platon and Sen Gupta, 2001;

Barmawidjaja et al., 1992; Gooday & Hughes, 2002; Langezaal et al., 2006; Duchemin et al., 2007; Mojtahid et al., 2008; Tichenor et al., 2016). Some studies suggest that *E. vitrea* are transported by the Mississippi River-induced currents and its presence instead indicates the extent of the Mississippi River discharge plume (Blackwelder et al., 1996; Platon and Sen Gupta, 2001). Additionally, high abundances have been attributed to increased sediment input causing the seasonal upward migration of *E. vitrea* (Barmawidjaja et al., 1992). Lastly, *E. vitrea* could be responding to high inputs of phytodetritus (Gooday & Hughes, 2002; Langezaal et al., 2006; Duchemin et al., 2007; Mojtahid et al., 2008). Thus, if the percent abundance of *E. vitrea* dominates the PEB and PEBn index, then the index could be reflecting changes in sedimentation rate stemming from delta progradation rather than hypoxia (Tichenor et al., 2016). Since my study area was not within range of nearby river delta progradation (Suter and Berryhill, 1985; Abdulah et al., 2004) and counts of my samples show that PEB and PEBn taxa are not dominated by *E. vitrea*, I consider the PEB and PEBn index to be feasible indicators of hypoxia in this study.

Osterman et al., (2006) grouped the morphically similar *N. opima* with *P. atlanticum*. The grouping of these morphologically similar taxa (herein known as the PEBn) was followed by Tichenor et al. (2016). My results suggest that PEBn records the same temporal patterns as the PEB in the offshore core, suggesting that the addition of *N. opima* does not influence the hypoxia record in the offshore core. In the nearshore core, PEB and PEBn trends do not deviate until an abrupt PEBn increase at 50 cm (Figure 7a). This deviation may be due to *N. opima* being more tolerant of salinity fluctuations than *P. atlanticum* in the nearshore location, indicated by *N. opima* having more positive PCO 2 axis scores.

The A-E index is commonly used in water depths <30 m on the Louisiana Shelf, owing to the absence or scarcity of *Ammonia* and *Elphidium* at depths >30 m (Platon and Sen Gupta, 2001). However, A-E taxa are common and abundant on the Texas Shelf at depths of 84-100 m, as suggested by a downcore A-E study on the Texas Shelf near Matagorda Bay (Osterman et al., 2000). The A-E index is particularly useful for environments of fluctuating salinities, unlike the PEB index (Platon and Sen Gupta, 2001). For example, a recent study used the A-E index to reconstruct the paleo-hypoxic record near the Brazos River delta on the Texas Shelf, which is an environment prone to salinity fluctuations (Strauss et al., 2012). They found that low-oxygen conditions, as indicated by A-E index values > 60%, persisted since the 1960s. Variations in the A-E index were coupled with fluctuations in Brazos River discharge with dramatically low A-E (< 30%) values coinciding with past droughts in Texas. The coupling of the A-E index and Brazos River discharge suggest that hypoxia on the Texas Shelf is heavily influenced by freshwater input and associated stratification (Strauss et al., 2012). Since *Ammonia* and *Elphidium* are present and abundant in the nearshore core and the offshore core, the A-E was considered a viable hypoxia proxy for the Texas Shelf near Mustang Island, TX.

4.3. Hypoxic Conditions Indicated by Foraminiferal Indices

The foraminiferal indices in both cores studied here show that hypoxia is present on the Texas Shelf. Most samples in the offshore core have PEB and PEBn values above >7%, which is the modern Texas Shelf hypoxia threshold defined by Osterman et al. (2004), whereas only a few samples with PEB and PEBn values >7% are seen in the nearshore core. This suggests that the offshore core has experienced more frequent hypoxic conditions than the nearshore core. In the offshore core, PEBn values remain above the record's mean value since ~127 cm core depth, and

A-E values have remained above the A-E mean since 51 cm. Both indices suggest that hypoxic conditions near the offshore core have become more severe towards the modern. In the nearshore core, PEBn values cross the mean value six times after 240 cm but cross the record more frequently in the upper 43 cm of the core (3 of the 4 samples cross the record after 43 cm). The A-E index, which may perform better in low-saline conditions, had values that remain above the mean value since 40 cm in the nearshore core, indicating that oxygen is lower in the last 40 cm than earlier in the record. The hypoxia indices in the nearshore core do not record analogous hypoxia signals in the upper portion of the core. Abundances of the PEB taxa in this core may have been reduced by salinity fluctuations and thus this index could not record hypoxic conditions from 41 cm to the core top. Thus, there may be a decoupling of the PEB and A-E index in the nearshore core during periods of increased runoff.

4.4. Sedimentation Rates and the Timing of Hypoxic Events

The SARs inferred from the $^{210}Pb_{xs}$ in the offshore core was higher than the nearshore core. The upper 8 cm of both cores represent the depth of the mixed layer, as indicated by uniform $^{210}Pb_{xs}$ activity throughout this section of the core. The offshore ^{210}Pb samples yielded only a 20-year chronology and the deeper part of the core is assumed to have the same SAR for age estimates. The two SARs derived from the nearshore ^{210}Pb activities may reflect recent slumping of older sediments on top of younger sediments – characteristic of physical mixing from flooding. Due to the mixing in the nearshore core, there are greater uncertainties in the extrapolated ages of the older portions of the core that were derived from the SARs. Moreover, the approximated ages derived from the extrapolated SARs in either core could be younger or older, if sedimentation rates in the past were higher or lower, respectively.

4.4.1. Offshore core: Synchronous Stepped Change in Oxygenation Indices

Time-series model selection suggests that the best supported model for PEB, PEBn and A-E change in the offshore core is an abrupt shift, preceded by and followed by periods of stasis. The step model suggests that all three foraminiferal oxygen indices in the offshore core abruptly increased, signifying a decrease in oxygen, at 51 cm. The ^{210}Pb ages suggest these shifts occurred at ~2000 CE (CI: 1992-2003 CE). After the shift, PEB and PEBn values remain above 6% and 8%, respectively, and A-E values remain exclusively above its mean in the record. A shift in richness and evenness overlaps the shift seen in the foraminiferal indices. Both richness and evenness shift to lower values at 10 cm or ~2016 CE (CI: 2015-2016 CE), indicating that either environmental stresses began to affect community structure (Murray, 2006) or more sediment input during this time.

The ~2000 CE (CI: 1992-2003 CE) shift indicated by the foraminiferal indices may coincide with the 2002 flooding of the Nueces River where the annual discharge was 2,743 ft^3/s (USGS River Gage 8211000, http:// waterdata.usgs.gov), which is the highest river discharge on the Nueces River since direct discharge measurements began in 1962. This is consistent with the hypothesis that hypoxia on the Texas Shelf is driven by high freshwater discharge, as suggested by DiMarco et al. (2012). However, high flow of the Nueces River does not persist after 2002, and hypoxic conditions after 2002 are more consistent with the expansion of the Louisiana Shelf hypoxic zone. The estimated areal extent of bottom-water hypoxia in the Gulf of Mexico, reached record highs in 2001 and 2002 (>20,000 km^2) and remain above the environmental baseline (>5,000 km^2) until 2019, except during drought and hurricane events (Rabalais and

Turner, 2019). Thus, the persistent hypoxic conditions after ~2002 may be due to increased freshwater flux from the Mississippi-Atchafalaya Rivers rather than the Nueces River.

Prior to this abrupt shift, PEBn values were above the mean value of 13.5% between 127 and 51 cm in the offshore core, suggesting that hypoxia was present if I use the definition of Osterman (2003) — PEB > 7% is indicative of modern-day hypoxia. If I assume a constant sedimentation rate, hypoxic conditions may have begun in ~1970 CE (CI: 1949-1977 CE) at this site and subsequently shifted to more severe conditions at ~2000 CE (CI: 1992-2003 CE). The oxygenation record in the offshore core overlaps with the oxygenation history of the Mississippi-Louisiana coast where dead zones have been expanding since the 1950s as indicated by elevated PEB and A-E index values (Osterman et al., 2009).

4.4.2. Nearshore core: Stepped Change in Oxygenation and Decoupling of AE and PEB Indices

The best supported time-series model for the nearshore PEB and PEBn change indicates an abrupt increase at 240 cm preceded by and followed by intervals of stasis. If I assume a constant SAR, this shift occurred at ~1600 CE (CI: 1471-1691 CE). However, this deeper shift is likely an artifact of the sampling resolution. The more recent hypoxic event in the nearshore core is characterized by a punctuated increase in PEBn at ~1950 CE (CI: 1925-1963 CE), and values continue to remain above the mean value of the record until the youngest sample. Abrupt hypoxic events prior to anthropogenic disturbance have been reported (Osterman et al., 2008) and may explain why shifts in the PEB occur near ~1600 CE (CI: 1471-1691 CE). PEB and PEBn values do not remain above 7% after 1950 CE (CI: 1925-1963 CE) and a shift is not

supported at this interval, which may be due PEBn taxa being sensitive to more frequent salinity fluctuations in the nearshore core (Platon and Sen Gupta, 2001).

For the A-E time-series, the best supported model indicates an abrupt increase at 40 cm preceded by and followed by intervals of stasis. The ^{210}Pb ages suggest these shifts occurred at ~1950 CE (CI: 1925-1963 CE). After 40 cm, A-E values increase until 3 cm, and is statistically supported as a shift to higher index values. The shift to more hypoxic conditions after 1950 CE (CI: 1925-1963 CE) is consistent with A-E studies on the Louisiana Shelf (Sen Gupta and Platon, 2004). The A-E, PEB and PEBn indices do not record analogous hypoxia shifts and may be decoupled due to the A-E taxa being tolerant to a wide salinity range at the nearshore location (Platon and Sen Gupta, 2001). The best supported model for both richness and evenness is stasis, suggesting a static value throughout the entire core. Thus, richness and evenness values have remained static throughout the nearshore record.

4.5. Faunal Gradients Defined by Oxygenation and Salinity

The multivariate ordination analysis allowed me to determine if there were other genera that covary with PEB or A-E index taxa and thus should also be considered in paleo-oxygenation studies of the GoM. Ordination analyses can also create more informative oxygenation scales for comparing the relative severity of hypoxia than index taxon methods (Sharon et al., 2021). Sample position on PCO axis 1 was primarily influenced by hypoxia tolerant and intolerant taxa. Negative scores were associated with the taxa that make up the PEB and A-E indices in addition to other taxa, such as *Bulimina*, *Brizalina*, *Fursekonia* and *Cassidulina*, that are associated with low-oxygen conditions (Murray, 2006). Oxic taxa, including *Trioculina, Quinqueloculina* and *Pygro* (Kaiho et al., 2014; Sharon et al., 2021), had positive scores. Because PCO axis 1

correlates with all of the foraminiferal indices (PEB, PEBn and A-E index), this suggests that shifts in PCO1 scores is largely defined by oxygenation. Thus, the decrease in PCO axis 1 scores at the offshore site from ~100 cm to 5 cm (~1980 - ~2017; CI: 1964-2017) and at the nearshore site from ~50 cm to the core top (~1950 to 2019; CI: 1925-2019), reflects a shift to low-oxygen conditions. The sharp increase in PCO axis 1 scores from ~5 cm to the core top (~2017 - ~2019: CI: 2016-2019) in the offshore core is indicative of a more oxygenated period, which could be due to the mixing and associated oxygenation of the water column after a hurricane event (Rabalais 2007; Rabalais and Turner, 2019), such as Hurricane Harvey in 2017. This hurricane event induced high sediment input to the Texas coast, generating 22 cm of new sediment in Galveston Bay, Texas (Du et al., 2019), thus 5 cm of sediment input from Hurricane Harvey at the offshore site is plausible. This interpretation of the oxygenation history differs from that derived from the PEB and A-E indices due to PCO axis 1 accounting for other oxygen-sensitive genera that covary with PEB or A-E index taxa.

The PCO axis 2 scores reflect changes in salinity, with more positive scores being indicative of a less saline environment and negative scores reflecting more saline or marine environments. Most taxa in this study had negative scores, including *Cibicidoides* and *Cibicides* which dwell in normal marine conditions (Murray 2006), whereas taxa such as *Ammonia* and *Elphidium* that are associated with brackish environments and that can tolerate lower salinities (5-22 psu; Bock et al., 1971; Hayward et al., 2004) had positive scores. Additionally, the nearshore and offshore samples grouped in opposite ends of PCO axis 2, where the nearshore site samples were positive and offshore site samples were negative. Nearshore sites are closer to Aransas Pass, a water inlet that connects the hyposaline bay system of Corpus Christi (psu = 22; Gulfbase.org) to the open ocean, allowing nearshore sites to be more vulnerable to changes in

freshwater discharge. Although most offshore samples had negative PCO axis 2 scores, various offshore sites were positive, which may be attributed to freshwater reaching offshore sites. For example, the offshore sample at 51 cm (~2000 CE, CI: 1992-2003 CE) may have been influenced by the high flow of the Nueces River in 2002. Thus, the increase in PCO axis 2 scores in the offshore from ~120 cm to the core top suggests an increase in freshwater input based on the faunal gradients from ~1970 towards the present. In the nearshore core, PCO axis 2 scores gradually increase from 150 cm to the present, with an abrupt decrease at 50 cm. The ^{210}Pb ages suggest the decrease in value (decrease in freshwater input suggested by fauna) occurs near ~1950 CE (CI: 1925-1963 CE). This decrease in freshwater flux may reflect the Texas Drought of Record that occurred from 1948 to 1957-- the worst drought ever recorded in Texas (McGregor et al., 2015).

As suggested earlier, flux of freshwater input may cause a decoupling of the hypoxia indices, due to the A-E index taxa being euryhaline, unlike PEBn taxa (Platon and Sen Gupta, 2001). The ordination allowed me to compare where the offshore and nearshore sites occupy ordination space relative to hypoxia-tolerant and salinity-tolerant taxa and where the hypoxia indices plot relative to one another. Nearshore sites plot more proximal to euryhaline taxa whereas the offshore sites plot near normal-marine taxa. The ordination space that the nearshore sites occupy is more proximal to the A-E taxa ordination space than PEBn, whereas the ordination space that the offshore sites occupy overlaps with the PEBn and A-E taxa ordination space. This suggests that offshore sites are more likely to have both A-E and PEBn taxa present in the samples, whereas nearshore sites are more likely to have A-E taxa than PEBn taxa.

4.6. Relationship between Oxygen and Carbon Isotopes and Faunal Variables

Through the Loop Current of the Gulf of Mexico, water masses from the Mississippi-Atchafalaya Rivers extend into the Texas Shelf (Rabalais et al., 2001), thus the decrease in salinity may be a reflection in freshwater from the Nueces River and the Mississippi-Atchafalaya Rivers, exclusively or in combination. Based on the salinity changes derived from the two component models, the offshore site had a greater salinity change when assuming two-component mixing between the Nueces River and GoM than when assuming two-component mixing between the Mississippi River and GoM.

If the entire -0.4‰ $\delta^{18}O$ excursion at 49 cm in the offshore site is attributed to a change in freshwater influx, then that isotopic event represents a salinity decrease of 2.4 to 4.2 psu depending on the primary source (Nueces or Mississippi-Atchafalaya) of the freshwater. In the sample capturing the lowest $\delta^{18}O$ value in the offshore core, faunal composition is more consistent with a lower salinity environment (higher abundance of *Ammonia spp.* and *Elphidium* spp.), in contrast to the majority of the offshore core samples (Figure 7). This supports the interpretation that the low $\delta^{18}O$ value reflects a change in freshwater influx and may correspond to the 2002 Nueces flooding event (US Department of Commerce and NOAA, 2017). Other studies have supported a primary influence of locally sourced freshwater on coastal $\delta^{18}O$ values during periods of high flow of the Brazos River, Brazos River water was the most dominant source of freshwater, whereas normal or drought periods were associated with Mississippi river waters (Strauss et al. 2012; DiMarco et al., 2012). Further, during the Texas Drought of Record (TDR) from 1948 to 1957, $\delta^{18}O$ values increased by 0.6‰ near the Brazos Delta, which was associated with a salinity increase of ~ 6 psu (Strauss et al. 2012), thus the values I reconstruct are within the range expected for drought events.

The decrease in salinity in the offshore site also coincides with a shift to higher PEBn, lower A-E values, and higher PCO axis 1 scores, supporting an interaction between freshwater influx and hypoxia for this extreme event. Thus, if local freshwater discharge is dominant in this area during high flow events, hypoxic conditions may be dependent on drought and flooding periods in Texas. Future stable isotope studies of the Texas Shelf waters near Mustang Island, TX are essential for identifying and drawing conclusions on the dominant freshwater sources in the area, especially during flooding events.

Carbon isotopes record changes in the $\delta^{13}C$ of bottom water dissolved inorganic carbon (DIC), and organic matter remineralization in the sediments. Since *E. excavatum* is an infaunal taxon, lower $\delta^{13}C$ may reflect organic carbon remineralization in the pore waters. The $\delta^{13}C$ of *E. excavatum* in an estuarine environment recorded a decrease in values from the 1960s to 1990s, which was interpreted as an increase in benthic respiration and associated hypoxic conditions (Thomas et al., 2000). However, Mellon et al., 2019 found that exceptionally low $\delta^{13}C$ values in portions of their core after ~1950 CE are caused by the Suess Effect (change in the ratio of carbon isotopes due to an increase in fossil-fuel derived CO_2). Thus, *E. excavatum* $\delta^{13}C$ in the youngest part of the offshore record ($\delta^{13}C$ = -1.8‰ to -1.4‰) may be an artifact of the Suess Effect. There were no significant correlations between $\delta^{13}C$ and the foraminiferal indices or PCO values across the full timeseries at either site with/without the samples that may be confounded by the Suess Effect.

5. CONCLUSION

To better understand the history of Texas Shelf hypoxia and whether conditions are influenced by local river runoff, I use variation in benthic foraminiferal faunas from ^{210}Pb-dated sedimentary cores to assess the temporal extent and severity of hypoxia on the Texas Shelf. In the nearshore core, the low-oxygen conditions recorded during a major drought between 1948 to 1957 may have been driven by the extension of the Mississippi-Atchafalaya plume, as suggested by an abrupt decrease in freshwater input (indicated by PCO 2 axis scores) and spike in hypoxia (indicated by increase in the PEBn index). Following this drought, an increase in freshwater input (indicated by PCO axis 2 scores) and hypoxic conditions (indicated by PCO 1 axis scores and the A-E index) seem to occur simultaneously after ~1950. PEB and PEBn index do not record a shift in hypoxia during this period and may be due to the extirpation of species in lower saline waters.

In the offshore core, an increase in freshwater input coincides with an increase in hypoxic conditions near ~1970, as indicated by the PCO axis 2 and 1 scores, respectively. However, the increase in PCO axis 1 scores from ~1980 (CI: 1986-1964) to ~2017 (CI: 2016-2017) in the offshore core precedes the supported shifts in the PEB, PEBn and A-E values at ~2000 CE (CI: 1992-2003 CE). The offset in the foraminiferal index values and PCO axis 1scores suggests that other hypoxic taxa not considered in the foraminiferal indices are responding to hypoxic conditions on the Texas Shelf prior to the PEB, PEBn and A-E taxa. Thus, the other hypoxic taxa

defining the faunal gradient of PCO axis 1 should be considered in future paleo-oxygenation studies of the Texas Shelf.

Local Texas river discharge may play a major role in hypoxic conditions during flooding events. The low $\delta^{18}O$ value near the ~2000 CE (CI: 1992-2003 CE) event reflects a change in freshwater influx, which may correspond to the 2002 Nueces flooding event. However, future stable isotope studies are needed near Mustang Island, TX to better understand the water masses that affect this region during flooding and drought events.

REFERENCES

Andersen, H. V. (1961). Foraminifera of the mudlumps, lower Mississippi River Delta. In: Genesis and Paleontology of the Mississippi River Mudlumps: Louisiana Geol. Survey, Geol.Bull., 35(2), 208.

Bapst, D.W. (2012). paleotree: an R package for paleontological and phylogenetic analyses of evolution. Methods in Ecology and Evolution, 3(5), 803-807. https://doi.org/10.1111/j.2041-210X.2012.00223.x.

Barmawidjaja, D. M., Jorissen, F. J., Puskaric, S., & van der Zwaan, G. J. (1992). Microhabitat selection by benthic foraminifera in the northern Adriatic Sea. Journal of Foraminiferal Research, 22(4), 297–317. https://doi.org/10.2113/gsjfr.22.4.297.

Bauch, H.A., Erlenkeuser, H., Bauch, D., Müller-Lupp, T. and Taldenkova, E. (2004). Stable oxygen and carbon isotopes in modern benthic foraminifera from the Laptev Sea shelf: implications for reconstructing proglacial and profluvial environments in the Arctic. Marine Micropaleontology, 51(3-4), 285-300. https://doi.org/10.1016/j.marmicro.2004.01.002.

Blackwelder, P., Hood, T., Alvarez-Zarikian, C., Nelsen, T. A., & McKee, B. (1996). Benthic foraminifera from the NECOP study area impacted by the Mississippi River plume and seasonal hypoxia. Quaternary International, 31, 19–36. https://doi.org/10.1016/1040-6182(95)00018-E.

Bock, W.D., (1971). A handbook of the benthonic foraminifera of Florida Bay and adjacent waters. Miami Geological Society, Memoir, 1, 1-92.

Breitburg, D., Levin, L. A., Oschlies, A., Grégoire, M., Chavez, F. P., Conley, D. J., et al. (2018). Declining oxygen in the global ocean and coastal waters. Science, 359(6371). https://doi.org/10.1126/science.aam7240.

Brunner, C.A., Beall, J.M., Bentley, S.J. and Furukawa, Y. (2006). Hypoxia hotspots in the Mississippi Bight. The Journal of Foraminiferal Research, 36(2), 95-107. https://doi.org/10.2113/36.2.95.

Cushman, J.A. (1947). New species and varieties of Foraminifera from off the southeastern coast of the United States. Contributions from the Cushman Laboratory for Foraminiferal Research, 23(8).

David, M.B., Drinkwater, L.E. & McIsaac, G.F. (2010). Sources of nitrate yields in the Mississippi River Basin. Journal of environmental quality, 39(5), 1657-1667. https://doi.org/10.2134/jeq2010.0115.

Diaz, R. J., & Rosenberg, R. (2008). Spreading dead zones and consequences for marine ecosystems. Science, 321(5891), 926–929.

DiMarco, S., Strauss, J., May, N., Mullins-Perry, R., Grossman, E., & Shormann, D. (2012). Texas coastal hypoxia linked to Brazos River discharge as revealed by oxygen isotopes. Aquatic Geochemistry, 18(2), 159–181. https://doi.org/10.1007/s10498-011-9156-x

Duchemin, G., Fontanier, C., Jorissen, F.J., Barras, C. and Griveaud, C. (2007). Living small-sized (63–150 μm) foraminifera from mid-shelf to mid-slope environments in the Bay of Biscay. The Journal of Foraminiferal Research, 37(1), 12-32. https://doi.org/10.2113/gsjfr.37.1.12.

Du, J., Park, K., Dellapenna, T.M. & Clay, J.M., (2019). Dramatic hydrodynamic and sedimentary responses in Galveston Bay and adjacent inner shelf to Hurricane Harvey. Science of the Total Environment, 653(25), 554-564. https://doi.org/10.1016/j.scitotenv.2018.10.403.

Dutton, A., Wilkinson, B.H., Welker, J.M., Bowen, G.J. and Lohmann, K.C., (2005). Spatial distribution and seasonal variation in 18O/16O of modern precipitation and river water across the conterminous USA. Hydrological Processes: An International Journal, 19(20), 4121-4146.

Esri Inc. (2020). ArcGIS Pro (Version 2.5). Esri Inc. https://www.esri.com/enus/arcgis/products/arcgispro/overview.

Esri, Maxar, Earthstar Geographics, USDA FSA, USGS, Aerogrid, IGN, IGP, and the GIS User Community. “World Imagery” [base map]. Scale not given. December 12, 2009. https://services.arcgisonline.com/ArcGIS/rest/services/World_Imagery/MapServr. (May 14, 2021).

Hunt, G. (2006). Fitting and comparing models of phyletic evolution: random walks and beyond. Paleobiology, 32(4), 578-601. https://doi.org/10.1666/05070.1.

Hunt, G. (2019). paleoTS: Analyze Paleontological Time-Series. R package version 0.5.2. https://CRAN.R project.org/package=paleoTS

Gooday, A. J., & Hughes, J. A. (2002). Foraminifera associated with phytodetritus deposits at a bathyal site in the northern Rockall Trough (NE Atlantic): seasonal contrasts and a comparison of stained and dead assemblages. Marine Micropaleontology, 46(1–2), 83–110. https://doi.org/10.1016/S0377-8398(02)00050-6

Gooday, Andrew J., Bett, B. J., Escobar, E., Ingole, B., Levin, L. A., Neira, C., et al. (2010). Habitat heterogeneity and its influence on benthic biodiversity in oxygen minimum zones. Marine Ecology, 31(1), 125–147. https://doi.org/10.1111/j.1439-0485.2009.00348.x

GulfBase, Corpus Christi Bay(n.d.). https://www.gulfbase.org/geological-feature/corpus-christi-bay.

Gupta, B.S. and Platon, E. (2006). Tracking past sedimentary records of oxygen depletion in coastal waters: use of the Ammonia-Elphidium foraminiferal index. Journal of Coastal Research, 39, 1351-1355.

Gupta, B.S. and Platon, E. (2006). Tracking past sedimentary records of oxygen depletion in coastal waters: use of the Ammonia-Elphidium foraminiferal index. Journal of Coastal Research, 39, 1351-1355.

Hunt G, Roy K (2006) Climate change, body size evolution, and Cope's Rule in deep-sea ostracodes. Proceedings of the National Academy of Sciences 103(5), 1347-1352. https://doi.org/10.1073/pnas.0510550103.

Hurlbert, S.H., 1971. The nonconcept of species diversity: a critique and alternative parameters. Ecology, 52(4), 577-586. https://doi.org/10.2307/1934145.

Hypoxia Watch. (2020, April 8). Retrieved May 29, 2020, from http://www.ncei.noaa.gov/products/hypoxia-watch

IFADATA. (n.d.). Retrieved May 29, 2020, from http://ifadata.fertilizer.org/ucSearch.aspx

Jorissen, F. J., Fontanier, C., & Thomas, E. (2007). Paleoceanographical proxies based on deep-sea benthic foraminiferal assemblage characteristics. Developments in Marine Geology, 1, 263–325. https://doi.org/10.1016/S1572-5480(07)01012-3.

Justić, D., Rabalais, N. N., & Turner, R. E. (1995). Stoichiometric nutrient balance and origin of coastal eutrophication. Marine Pollution Bulletin, 30(1), 41–46. https://doi.org/10.1016/0025-326X(94)00105-I.

Keeling, R. F., Körtzinger, A., & Gruber, N. (2010). Ocean deoxygenation in a warming world. Annual Review of Marine Science, 2(1), 199–229. https://doi.org/10.1146/annurev.marine.010908.163855

Koesema, D. J., & Laskowski, N. A. (2019). Corpus Christi Ship Channel Improvement Project. USACE Galveston District Summer Stakeholder Partnering Forum. Galveston, TX. Retrieved May 29, 2020, from https://www.swg.usace.army.mil/Portals/26/09%20Stakeholder%20Meeting%2008-14-2019%20Final_1.pdf

Langezaal, A. M., Jorissen, F. J., Braun, B., Chaillou, G., Fontanier, C., Anschutz, P., & van der Zwaan, G. J. (2006). The influence of seasonal processes on geochemical profiles and foraminiferal assemblages on the outer shelf of the Bay of Biscay. Continental Shelf Research, 26(15), 1730–1755. https://doi.org/10.1016/j.csr.2006.05.005

Lee, D.H., Veizer, J., (2003). Water and carbon cycles in the Mississippi River basin: potential implications for the Northern Hemisphere residual terrestrial sink. Global Biogeochemical Cycles, 17. http://dx.doi.org/10.1029/ 2002GB001984.

Legendre, P. & Legendre, L. (2003). Numerical Ecology, Volume 24—3rd Edition, second English edition. Developments in Environmental Modelling, Elsevier: Amsterdam, Netherlands, 20.

May, N.L & NOAA Southeast Fisheries Science Center (2016). Temperature, salinity, dissolved oxygen, and other measurements collected using CTD from NOAA Ship OREGON II in Gulf of Mexico from 2016 as part of the Southeast Area Monitoring and Assessment Program (SEAMAP) (NCEI Accession 0156169). NOAA National Centers for Environmental Information. Dataset. https://www.ncei.noaa.gov/archive/accession/0156169. Accessed May 6, 2021.

May, N.L. & NOAA Southeast Fisheries Science Center (2019). Temperature, salinity, dissolved oxygen measurements collected using CTD, bottle from multiple platforms in the Gulf of Mexico from 2009 through 2015 as part of the Southeast Area Monitoring and Assessment Program (SEAMAP) (NCEI Accession 0131259). NOAA National Centers for Environmental Information. Dataset. https://www.ncei.noaa.gov/archive/accession/0131259. Accessed May 6, 2021.

May, N.L. & NOAA Fisheries (2011). Temperature, salinity, dissolved oxygen measurements collected using CTD, bottle from multiple platforms in the Gulf of Mexico from 1992 through 2008 as part of the Southeast Area Monitoring and Assessment Program (SEAMAP) (NCEI Accession 0069702). NOAA National Centers for Environmental Information. Dataset. https://www.ncei.noaa.gov/archive/accession/0069702. Accessed May 6, 2021.

McCorkle, D.C., Corliss, B.H., & Farnham, C.A. (1997). Vertical distributions and stable isotopic compositions of live (stained) benthic foraminifera from the North Carolina and California continental margins. Deep Sea Research Part I: Oceanographic Research Papers, 44(6), 983-1024.

McGregor, K.M. (2015). Comparison of the recent drought in Texas to the drought of record using reanalysis modeling. Papers in Applied Geography, 1(1), 34-42. https://doi.org/10.1080/23754931.2015.1009295.

Mellon, S., Kienast, M., Algar, C., de Menocal, P., Kienast, S.S., Marchitto, T.M., Moros, M. and Thomas, H., 2019. Foraminifera trace anthropogenic CO2 in the NW Atlantic by 1950. Geophysical Research Letters, 46(24), 14683-14691.

Mojtahid, M., Jorissen, F. and Pearson, T.H. (2008). Comparison of benthic foraminiferal and macrofaunal responses to organic pollution in the Firth of Clyde (Scotland). Marine Pollution Bulletin, 56(1), 42-76. https://doi.org/10.1016/j.marpolbul.2007.08.018

Murray, J.W. (2006). Ecology and applications of benthic foraminifera. Cambridge university press.

Nelsen, T. A., Blackwelder, P., Hood, T., McKee, B., Romer, N., Alvarez-Zarikian, C., & Metz, S. (1994). Time-based correlation of biogenic, lithogenic and authigenic sediment components with anthropogenic inputs in the Gulf of Mexico NECOP study area. Estuaries, 17(4), 873–885. https://doi.org/10.2307/1352755

Nittrouer, C.A., Sternberg, R.W., Carpenter, R. and Bennett, J.T. (1979). The use of Pb-210 geochronology as a sedimentological tool: application to the Washington continental shelf. Marine Geology, 31(3-4), 297-316. https://doi.org/10.1016/0025-3227(79)90039-2.

Oksanen, J., Blanchet, F.G., Friendly, M., Kindt,R., Legendre,P., McGlinn,D., Minchin,P.R., O'Hara, R. B. , Simpson, G.L., Solymos, P., Stevens, M.H.H., Szoecs, E., & Wagner, H. (2020). vegan: Community Ecology Package. R package version 2.5-7. https://CRAN.R project.org/package=vegan

Olivera, F., & DeFee, B. B. (2007). Urbanization and its effect on runoff in the Whiteoak Bayou Watershed, Texas. JAWRA Journal of the American Water Resources Association, 43(1), 170–182. https://doi.org/10.1111/j.1752-1688.2007.00014.x

Osterman, L. E. (2003). Benthic foraminifers from the continental shelf and slope of the Gulf of Mexico: an indicator of shelf hypoxia. Estuarine, Coastal and Shelf Science, 58(1), 17–35. https://doi.org/10.1016/S0272-7714(02)00352-9

Osterman, L. E., Erlandsen, M., & Castensin, E. D. (2001). Benthic foraminiferal census data from surface sediment samples, western Gulf of Mexico (Louisiana and Texas continental shelf and slope). U.S. Geological Survey Open File, 1-182.

Paramasivam, C.R. and Venkatramanan, S. (2019). An introduction to various spatial analysis techniques. GIS and Geostatistical Techniques for Groundwater Science, edited by:Venkatramanan, S., Prasanna, MV, and Chung, SY, Elsevier, Amsterdam, the Netherlands, 23-30.

Phleger, F. B., & Parker, F. L. (1951). Ecology of Foraminifera, Northwest Gulf of Mexico. Part II. Foraminiferal species. Geological Society America Memoir 46.

Phleger, F.B. (1953). North Atlantic core foraminifera. Reports on the Swedish Deep-Sea Expedition, 1-122.

Platon, E., & Gupta, B. K. S. (2013). Benthic foraminiferal communities in oxygen-depleted environments of the Louisiana continental shelf. In Coastal Hypoxia: Consequences for Living Resources and Ecosystems. American Geophysical Union (AGU), 58, 147–163 https://doi.org/10.1029/CE058p0147

Poag, C.W., (2015). Benthic foraminifera of the Gulf of Mexico: distribution, ecology, paleoecology. Texas A&M University Press.

Polyak, L., Stanovoy, V. & Lubinski, D.J. (2003). Stable isotopes in benthic foraminiferal calcite from a river-influenced Arctic marine environment, Kara and Pechora Seas. Paleoceanography, 18(1). https://doi.org/10.1029/2001PA000752.

Port of Corpus Christi (2019). Annual Report 2018-2019. Available at: https://portofcc.com/wpcontent/uploads/2018-Annual-Report-1.pdf (Accessed: 6 May 2021)

Purcell, K. M., Craig, J. K., Nance, J. M., Smith, M. D., & Bennear, L. S. (2017). Fleet behavior is responsive to a large-scale environmental disturbance: Hypoxia effects on the spatial dynamics of the northern Gulf of Mexico shrimp fishery. PLOS ONE, 12(8), https://doi.org/10.1371/journal.pone.0183032

R Core Team (2021). R: A language and environment for statistical computing. R Foundation for Statistical Computing, Vienna, Austria. URL https://www.R-project.org/.

Rabalais, N.N. and Turner, R.E. (2019). Gulf of Mexico hypoxia: Past, present, and future. Limnology and Oceanography Bulletin, 28(4), 117-124. https://doi.org/10.1002/lob.10351.

Rabalais, N. N., Díaz, R. J., Levin, L. A., Turner, R. E., Gilbert, D., & Zhang, J. (2010). Dynamics and distribution of natural and human-caused hypoxia. Biogeosciences, 7(2), 585–619. https://doi.org/10.5194/bg-7-585-2010

Rabalais, N. N., Turner, R. E., Sen Gupta, B. K., Boesch, D. F. , Chapman, P. & Murrell, M. C. (2007). Characterization and long- term trends of hypoxia in the northern Gulf of Mexico: Does the science support the action plan? Estuar. Coasts 30(5), 753–772. https://doi.org/10.1007/bf02841332.

Rabalais, N.N., Turner, R.E. & Wiseman Jr, W.J. (2001). Hypoxia in the Gulf of Mexico. Journal of environmental quality, 30(2), 320-329. https://doi.org/10.2134/jeq2001.302320x.

Rabalais, Nancy N., & Baustian, M. M. (2020). Historical shifts in benthic infaunal diversity in the northern Gulf of Mexico since the appearance of seasonally severe hypoxia. Diversity, 12(2), 49. https://doi.org/10.3390/d12020049

Rabalais, Nancy N., Turner, R. E., & Wiseman, W. J. (2002). Gulf of Mexico Hypoxia, a.k.a. "The Dead Zone." Annual Review of Ecology and Systematics, 33, 235–263. https://doi.org/10.1146/annurev.ecolsys.33.010802.150513

Rabalais, Nancy N., Turner, R. E., Gupta, B. K. S., Platon, E., & Parsons, M. L. (2007). Sediments tell the history of eutrophication and hypoxia in the Northern Gulf of Mexico. Ecological Applications, 17(5), 129–143. https://doi.org/10.1890/06-0644.1

Rabalais, Nancy N., Turner, R. E., Justić, D., Dortch, Q., Wiseman, W. J., & Gupta, B. K. S. (1996). Nutrient changes in the Mississippi River and system responses on the adjacent continental shelf. Estuaries, 19(2), 386–407. https://doi.org/10.2307/1352458

Sanders, H.L. (1968). Marine benthic diversity: a comparative study. The American Naturalist, 102(925), 243-282.

Santschi, P.H., Guo, L., Asbill, S., Allison, M., Kepple, A.B. and Wen, L.S. (2001). Accumulation rates and sources of sediments and organic carbon on the Palos Verdes shelf based on radioisotopic tracers (137Cs, 239,240 Pu, 210Pb, 234Th, 238U and 14C). Marine Chemistry, 73(2), 125-152. https://doi.org/10.1016/S0304-4203(00)00101-8.

Schmittner, A., Oschlies, A., Matthews, H.D. & Galbraith, E.D. (2008). Future changes in climate, ocean circulation, ecosystems, and biogeochemical cycling simulated for a business-as-usual CO2 emission scenario until year 4000 AD. Global biogeochemical cycles, 22(1). https://doi.org/10.1029/2007GB002953.

Sen Gupta, B. K., Turner, R. E., & Rabalais, N. N. (1996). Seasonal oxygen depletion in continental-shelf waters of Louisiana: Historical record of benthic foraminifers. Geology, 24(3), 227–230. https://doi.org/10.1130/0091-7613(1996)024<0227: SODICS>2.3.CO;2

Sheng, J., & Wilson, J. P. (2009). Watershed urbanization and changing flood behavior across the Los Angeles metropolitan region. Natural Hazards, 48(1), 41–57. https://doi.org/10.1007/s11069-008-9241-7

Smith, M. D., Asche, F., Bennear, L. S., & Oglend, A. (2014). Spatial-dynamics of hypoxia and fisheries: the case of Gulf of Mexico brown shrimp. Marine Resource Economics, 29(2), 111–131. https://doi.org/10.1086/676826

Smith, M. D., Oglend, A., Kirkpatrick, A. J., Asche, F., Bennear, L. S., Craig, J. K., & Nance, J.M. (2017). Seafood prices reveal impacts of a major ecological disturbance. Proceedings of the National Academy of Sciences,114(7), 1512-1517. https://doi.org/10.1073/pnas.1617948114

Stramma, L., Johnson, G.C., Sprintall, J., & Mohrholz, V. (2008). Expanding oxygen-minimum zones in the tropical oceans. Science, 320(5876), 655-658. https://doi.org/10.1126/science.1153847

Strauss, J., Grossman, E. L., Carlin, J. A., & Dellapenna, T. M. (2012). 100 Years of benthic foraminiferal history on the inner Texas shelf inferred from fauna and stable isotopes: Preliminary results from two cores. Continental Shelf Research, 38, 89–97. https://doi.org/10.1016/j.csr.2012.03.004

Suriya, S. and Mudgal, B.V. (2012). Impact of urbanization on flooding: The Thirusoolam sub watershed–A case study. Journal of hydrology, 412, 210-219. https://doi.org/10.1016/j.jhydrol.2011.05.008

Sutter, J.R. and Berryhill, H.L. (1985). Late Quaternary shelf-margin deltas, northwest Gulf of Mexico. AAPG Bulletin, 69(1), 77-91.

Swarzenski, P.W., Campbell, P.L., Osterman, L.E. and Poore, R.Z. (2008). A 1000-year sediment record of recurring hypoxia off the Mississippi River: The potential role of terrestrially-derived organic matter inputs. Marine Chemistry, 109(1-2), 130-142. https://doi.org/10.1016/j.marchem.2008.01.003.

Whitehurst, T., (2019). How can a canal full of water reduce flooding on Corpus Christi's North Beach?. Retrieved June 14, 2021, from https://www.caller.com/story/news/2019/07/11/how-can-canal-full-water-protect-north-beach-lets-take-look/1704343001/.

Thomas, E., Gapotchenko, T., Varekamp, J.C., Mecray, E.L. & Ten Brink, M.B. (2000). Benthic foraminifera and environmental changes in Long Island Sound. Journal of Coastal Research, 16(3), 641-655.

Tichenor, H. R., Culver, S. J., Corbett, D. R., Walsh, J. P., & Buzas, M. A. (2016). Does the PEB index respond only to hypoxia in the Mississippi Delta, Gulf of Mexico? Journal of Foraminiferal Research, 46(1), 48–60. https://doi.org/10.2113/gsjfr.46.1.48

Tourment, R., Wallis, M., Beullac, B., Kortenhaus, A., Schaaf, D.M. and Schelfhout, H. (2014), April. The risk analysis of levee systems. In 3rd IAHR Europe Congress, 13.

Turner, R. E., & Rabalais, N. N. (1991). Changes in Mississippi River water quality this century. BioScience, 41(3), 140–147. https://doi.org/10.2307/1311453.

US Department of Commerce, N. O. A. A. (2017). Disastrous River Flooding - June 30 Through July 17, 2002. National Weather Service. https://www.weather.gov/crp/20020717_Flood.

US DOC, NOAA, National Marine Fisheries Service, US DOC, NOAA, NESDIS, & National Centers for Environmental Information (2017). Water temperature, salinity, dissolved oxygen, and other measurements from CTD taken from NOAA Ship Oregon II in the Gulf of Mexico from 2017-06-09 to 2017-07-19 as part of the Southeast Area Monitoring and Assessment Program (SEAMAP) (NCEI Accession 0166524). NOAA National Centers for Environmental Information. Dataset. https://www.ncei.noaa.gov/archive/accession/0166524. Accessed May 6, 2021.

US DOC, NOAA, National Marine Fisheries Service; US DOC, NOAA, NESDIS, National Centers for Environmental Information (2018). Water temperature, salinity, dissolved oxygen, and other measurements from CTD taken from NOAA Ship Oregon II in the Gulf of Mexico from 2018 06-10 to 2018-07-19 as part of the Southeast Area Monitoring and Assessment Program (SEAMAP) (NCEI Accession 0174810). NOAA National Centers for Environmental Information. Dataset. https://www.ncei.noaa.gov/archive/accession/0174810. Accessed May 6, 2021.

USGS Current Conditions for USGS 08114000 Brazos River at Richmond, TX. (n.d.). Retrieved May 29, 2020, from https://waterdata.usgs.gov/usa/nwis/uv?08114000.

USGS Current Conditions for USGS 08116650 Nueces River at Rosharon, TX. (n.d.). Retrieved May 29, 2020, from https://waterdata.usgs.gov/tx/nwis/uv?site_no=08116650.

USGS (2015). Tracking water quality of the nation's rivers and streams. Accessed November 30, 2015. http://cida.usgs.gov/quality/rivers.

Vaquer-Sunyer, R., & Duarte, C. M. (2008). Thresholds of hypoxia for marine biodiversity. Proceedings of the National Academy of Sciences, 105(40), 15452–15457.

Weng, Q. (2001). Modeling urban growth effects on surface runoff with the integration of remote sensing and GIS. Environmental Management, 28(6), 737–748. https://doi.org/10.1007/s002670010258

World Population Prospects - Population Division - United Nations. (n.d.). Retrieved May 29, 2020, from https://population.un.org/wpp/Download/Standard/Population/.

Yang, L., Smith, J. A., Baeck, M. L., Bou-Zeid, E., Jessup, S. M., Tian, F., & Hu, H. (2013). Impact of urbanization on heavy convective precipitation under strong large-scale forcing: a case study over the Milwaukee–Lake Michigan Region. Journal of Hydrometeorology, 15(1), 261–278. https://doi.org/10.1175/JHM-D-13-020.1

Zhao, G., H., Gao, & L., Cuo (2016). Effects of urbanization and climate change on peak flows over the San Antonio River Basin, Texas. Journal of Hydrometeorology, 17(9), 2371 2389. https://doi.org/10.1175/JHM-D-15-0216.1

APPENDIX A

RAW GENUS-LEVEL COUNTS

Site ID	Depth (cm)	*Bigenerina*	*Ammodiscus*	*Ammonia*	*Angulogerina*	*Astrononion*	*Bifarina*	*Brizalina*	*Buccella*	*Bulimina*	*Buliminella*	*Cassidulina*	*Cancris*	*Cibicides*	*Cibicidoides*	*Cribrostomoides*
PC2 S1 0-2	2	7		188			1	1		0	1			1		2
PC2 S1 5-7	7	5		46				0		0	1					
PC2 S1 8-10	10	16		142			4	11	3	21	73			1		
PC2 S1 18-20	20	3		43				2	3	0	5					
PC2 S1 33-35	35	4		53			1	2	1	0	3					
PC2 S1 39-41	41	1		45			3	9	2	6	5	4				
PC2 S1 43-45	45	5		74				7	3	6	11					
PC2 S1 47-49	49	2		28				0		0	0					
PC2 S1 49-51	51			38				2		1	1					
PC2 S1 66-68	68	7		63				0	1	1	0					
PC2 S1 78-80	80			44				5	10	18	3				3	
PC2 S1 88-90	90	8		42				0		0	2					
PC2 S1 98-100	100	5		37				0	1	0	1		1			
PC2 S1 109-111	111	5	1	39			1	2		4	4		1			
PC2 S1 119-121	121	11		81			2	3		1	0					
PC2 S1 125-127	127	10		37				0		0	0					
PC2 S2 3-5	133	9		60				9	1	3	14			2		
PC2 S2 23-25	153	8		41			3	9	2	13	1	1	2	4	1	
PC2 S2 53-55	183	10		27				0		2	0					
PC2 S2 73-75	203	19		46			1	17	2	5	4					
PC2 S2 103-105	233	14		34				0		0	0		3	3		
PC2 S3 9-11	289	21		44				2	2	0	0					
PC2 S3 56-58	336	12		86				1	2	0	3		2			
PC2 S3 66-68	346	4		19	1		4	2	2	0	0		2		2	
PC2 S3 89-91	369	12		90			3	9	7	2	0		1			
PC2 S3 109-111	389	3		15				0		0	0		1			
PC2 S3 139-141	419	6		32				5		0	1					
PC3 S1 3-5	5	3		87				0		0	0					

PC3 S1 23-25	25	7		106				2	1	1	0					
PC3 S1 38-40	40	6		92				0		0	0					
PC3 S1 41-43	43	10		51				2		0	0					
PC3 S1 48-50	50	5		50				1	3	0	0					
PC3 S1 83-85	85	19		81				0		0	0					
PC3 S1 131-133	133	1		43				0	3	0	0					
PC3 S1 151-153	153	18		89				0		0	0		1			
PC3 S2 43-45	222	14		43		4		2	6	1	0					
PC3 S2 61-63	240	4		69				0		0	0			1		
PC3 S2 81-83	260	12		54				0		0	0					
PC3 S2 101-103	280	9	1	20				0		0	0					
PC3 S2 123-125	302	19		42				1		0	0					
PC3 S2 143-145	322	7		30				0		0	0					

Site ID	Depth (cm)	*Karreriella*	*Elphidium*	*Epistominella*	*Fissurina*	*Fursenkonia*	*Hanzawai*	*Saccammina*	*Lagena*	*Pseudononion*	*Nonionella*	*Melonis*	*Planulina*	*Pygro*	*Quinqueloculina*	*Milliamina*
PC2 S1 0-2	2	38	197	1		2	16			6	15				1	
PC2 S1 5-7	7		92	2		0	8				2		6		1	
PC2 S1 8-10	10		155	24		9	10				36				1	
PC2 S1 18-20	20		52	14		7	6			7	10				2	
PC2 S1 33-35	35		56	9		8	8			3	5	1			3	
PC2 S1 39-41	41		28	19	3	14	1		2	7	23	3			0	
PC2 S1 43-45	45		65	13		3	13			15	10				5	
PC2 S1 47-49	49		40	2		5	5		1	6	1				2	
PC2 S1 49-51	51		24	1		0	5			15	10				1	
PC2 S1 66-68	68		95	3		2	11				6		3		2	
PC2 S1 78-80	80		120	12		17	17		2	24	30				0	
PC2 S1 88-90	90		87	2		9	20	1		4	2				6	1
PC2 S1 98-100	100		100	2		0	18	1		10	5				13	
PC2 S1 109-111	111		82	5		6	9			18	6				3	1

PC2 S1 119-121	121		117	11		4	10	1		19	32			10	1
PC2 S1 125-127	127		71			0	7	1		11	1			2	
PC2 S2 3-5	133		62	31		21	5			6	2		1	7	1
PC2 S2 23-25	153		71	11		10	6	1		4	9			2	
PC2 S2 53-55	183		65	4		0	26			16				4	7
PC2 S2 73-75	203		139	9		7	34	2			32	23		3	
PC2 S2 103-105	233		71	5		3	21			11	5			3	8
PC2 S3 9-11	289		84	3		4	38	1		22	8			6	1
PC2 S3 56-58	336		105	10		3	26	1		11	3			5	
PC2 S3 66-68	346		65	2		4	13		1	13				0	
PC2 S3 89-91	369		124	3		2	66			20	5		1	10	5
PC2 S3 109-111	389		63	1		1	22			3	7		1	19	7
PC2 S3 139-141	419		60	4		5	9			10	1		1	12	11
PC3 S1 3-5	5	1	39			0	7			2	8			0	
PC3 S1 23-25	25		60			0	4			9	4			2	
PC3 S1 38-40	40		127			2	12			8	9	1		7	
PC3 S1 41-43	43		85			0	4			7	51			61	
PC3 S1 48-50	50		81			1	5				6	6		6	
PC3 S1 83-85	85		137			0	15					1		16	
PC3 S1 131-133	133		62			0	9			10	1			7	
PC3 S1 151-153	153		126			0	22			11	2	1	1	9	
PC3 S2 43-45	222		82	1		1	3	1		15	8			15	
PC3 S2 61-63	240		122			0	4			12	3			4	
PC3 S2 81-83	260		94			0	3			4	4		1	22	
PC3 S2 101-103	280		70			0	3			2	2			30	
PC3 S2 123-125	302		81			0				3	5			31	
PC3 S2 143-145	322		74			0				1	4			14	

Site ID	Depth (cm)	*Reussella*	*Rosalina*	*Sigmoilina*	*Textularia*	*Triloculina*	*Uvigerina*	Total Abundance
PC2 S1 0-2	2	2	0		0			479
PC2 S1 5-7	7		1		0			164
PC2 S1 8-10	10	12	0		0			518
PC2 S1 18-20	20	7	0		0			161
PC2 S1 33-35	35	3	0		1			161
PC2 S1 39-41	41		0		1			176
PC2 S1 43-45	45		0		12			242
PC2 S1 47-49	49	1	0		0			93
PC2 S1 49-51	51		0		3			101
PC2 S1 66-68	68		6	2	12			214
PC2 S1 78-80	80		0		0			305
PC2 S1 88-90	90	1	0		12			197
PC2 S1 98-100	100	2	0		5			201
PC2 S1 109-111	111	4	0		2			193
PC2 S1 119-121	121	3	0		2			308
PC2 S1 125-127	127	7	0		7			154
PC2 S2 3-5	133	6	0		24			264
PC2 S2 23-25	153	1	0		6			206
PC2 S2 53-55	183	8	0		12			181
PC2 S2 73-75	203		19		5			367
PC2 S2 103-105	233	14	0		18			213
PC2 S3 9-11	289	10	0		8			254
PC2 S3 56-58	336	13	0		15			298
PC2 S3 66-68	346	8	0		6			148
PC2 S3 89-91	369	20	0		21			401
PC2 S3 109-111	389	5	0		14			162
PC2 S3 139-141	419	4	0	1	10			172
PC3 S1 3-5	5		0		1			148
PC3 S1 23-25	25	1	0		0			197
PC3 S1 38-40	40	2	0		1			267
PC3 S1 41-43	43		0		3			274
PC3 S1 48-50	50		2	1	0			167
PC3 S1 83-85	85	2	0		1			272
PC3 S1 131-133	133		0		1			137
PC3 S1 151-153	153		0		1			281
PC3 S2 43-45	222	3	0	1	14			214

PC3 S2 61-63	240	4	0	0		223
PC3 S2 81-83	260		0	0		194
PC3 S2 101-103	280		0	0		137
PC3 S2 123-125	302	1	0	0		183
PC3 S2 143-145	322		0	0	1	131

APPENDIX B

LITHOLOGICAL, FAUNAL, AND GEOCHEMICAL DATA

Site	Depth (cm)	% Mud	$\delta^{13}C$	$\delta^{18}O$	PEB	PEB_N	A-E	PCO1	PCO2
PC2 S1 (0-2)	2	88.56	-1.76	-0.61	17.80	24.70	47.80	0.00	0.17

PC2 S1 (5-7)	7	86.20			6.30	8.30	45.40	0.09	0.14
PC2 S1 (8-10)	10	89.89			16.10	22.40	45.30	-0.20	0.04
PC2 S1 (18-20)	20	88.57	-1.40	-0.46	9.30	12.40	48.60	-0.16	-0.01
PC2 S1 (33-35)	35	98.53			17.40	30.30	61.60	-0.11	0.04
PC2 S1 (39-41)	41	49.35	-0.73	-0.41	16.10	20.20	53.20	-0.39	0.02
PC2 S1 (43-45)	45	86.47	-0.86	-0.91	8.60	9.70	41.20	-0.18	0.00
PC2 S1 (47-49)	49	78.99	-0.58	-0.47	16.80	26.70	61.30	0.00	0.05
PC2 S1 (49-51)	51	65.76	-0.86	-0.53	1.40	4.20	39.90	-0.20	0.07
PC2 S1 (66-68)	68	83.97	-0.80	-0.50	12.80	22.60	26.80	0.04	0.06
PC2 S1 (78-80)	80	83.98	-0.65	-0.46	4.10	5.10	32.60	-0.09	-0.10
PC2 S1 (88-90)	90	90.81	-1.33	-0.68	6.50	9.00	27.00	0.07	-0.06
PC2 S1 (98-100)	100	91.24	-0.87	-0.27	14.00	17.10	32.20	0.13	-0.03
PC2 S1 (109-111)	111	92.84	-0.95	-0.69	9.70	20.10	40.90	-0.01	-0.05
PC2 S1 (119-121)	121	70.29	-0.90	-0.09	7.10	7.80	34.30	-0.06	0.01
PC2 S1 (125-127)	127	94.31	-1.13	-0.74	19.30	20.10	49.20	0.09	-0.01
PC2 S2 (3-5)	133	89.50	-0.76	-0.48	7.80	12.10	36.60	-0.20	-0.11
PC2 S2 (23-25)	153	86.03	-1.11	-0.65	11.00	11.00	29.30	-0.12	-0.09
PC2 S2 (53-55)	183	84.20	-1.07	-0.41	3.30	12.00	24.90	0.07	-0.22
PC2 S2 (73-75)	203	82.54	-1.07	-0.23	7.50	9.90	32.40	-0.01	-0.12
PC2 S2 (103-105)	233	77.42	-1.44	-0.45	9.80	13.00	34.40	0.03	-0.20
PC2 S3 (9-11)	289	85.73	-1.14	-0.42	7.40	8.40	45.00	0.02	-0.17
PC2 S3 (56-58)	336	67.27	-0.58	-1.03	5.30	5.30	36.50	-0.03	-0.05
PC2 S3 (66-68)	346	88.17	-1.05	-0.44	10.10	10.10	22.60	0.08	-0.16
PC2 S3 (89-91)	369	88.17			5.70	7.00	42.10	-0.03	-0.14
PC2 S3 (109-111)	389	97.80	-0.56	-0.13	2.50	6.80	19.20	0.16	-0.19
PC2 S3 (139-141)	419	89.19	-0.72	-0.29	8.60	9.20	34.80	0.01	-0.14
PC3 S1 (3-5)	5	40.16	-1.10	-0.57	1.40	6.80	69.00	-0.14	0.20
PC3 S1 (23-25)	25	66.14	-1.41	-0.81	4.60	6.60	63.90	-0.10	0.15
PC3 S1 (38-40)	40	60.55	-0.58	-0.85	3.00	6.40	42.00	0.04	0.13
PC3 S1 (41-43)	43	85.07	-1.20	-0.39	2.60	21.20	37.50	0.01	-0.01
PC3 S1 (48-50)	50	37.81	-0.60	-0.58	0.00	3.60	38.20	0.06	0.14
PC3 S1 (83-85)	85				0.00	0.00	37.20	0.13	0.12
PC3 S1 (131-133)	133	85.77			7.30	8.00	41.00	0.06	0.08
PC3 S1 (151-153)	153	44.78			3.90	4.60	41.40	0.08	0.08
PC3 S2 (43-45)	222	80.59			7.50	11.20	34.40	0.05	-0.07
PC3 S2 (61-63)	240	64.43			5.40	6.70	36.10	0.07	0.14
PC3 S2 (81-83)	260	46.41			2.10	4.10	36.50	0.12	0.12
PC3 S2 (101-103)	280	35.02			1.50	2.90	22.20	0.25	0.04

PC3 S2 (123-125)	302	31.68			1.60	4.40	34.10	0.15	0.07
PC3 S2 (143-145)	322	31.68			0.80	3.80	28.80	0.17	0.11